PCCP

PAPER

View Article Online
View Journal | View Issue

Cite this: *Phys. Chem. Chem. Phys.*, 2014, **16**, 5349

The pyrolysis of 2-methylfuran: a quantum chemical, statistical rate theory and kinetic modelling study†

Kieran P. Somers,* John M. Simmie, Wayne K. Metcalfe and Henry J. Curran

Received 20th November 2013,
Accepted 27th January 2014

DOI: 10.1039/c3cp54915a

www.rsc.org/pccp

Due to the rapidly growing interest in the use of biomass derived furanic compounds as potential platform chemicals and fossil fuel replacements, there is a simultaneous need to understand the pyrolysis and combustion properties of such molecules. To this end, the potential energy surfaces for the pyrolysis relevant reactions of the biofuel candidate 2-methylfuran have been characterized using quantum chemical methods (CBS-QB3, CBS-APNO and G3). Canonical transition state theory is employed to determine the high-pressure limiting kinetics, $k(T)$, of elementary reactions. Rice–Ramsperger–Kassel–Marcus theory with an energy grained master equation is used to compute pressure-dependent rate constants, $k(T,p)$, and product branching fractions for the multiple-well, multiple-channel reaction pathways which typify the pyrolysis reactions of the title species. The unimolecular decomposition of 2-methylfuran is shown to proceed *via* hydrogen atom transfer reactions through singlet carbene intermediates which readily undergo ring opening to form collisionally stabilised acyclic C_5H_6O isomers before further decomposition to C_1–C_4 species. Rate constants for abstraction by the hydrogen atom and methyl radical are reported, with abstraction from the alkyl side chain calculated to dominate. The fate of the primary abstraction product, 2-furanylmethyl radical, is shown to be thermal decomposition to the *n*-butadienyl radical and carbon monoxide through a series of ring opening and hydrogen atom transfer reactions. The dominant bimolecular products of hydrogen atom addition reactions are found to be furan and methyl radical, 1-butene-1-yl radical and carbon monoxide and vinyl ketene and methyl radical. A kinetic mechanism is assembled with computer simulations in good agreement with shock tube speciation profiles taken from the literature. The kinetic mechanism developed herein can be used in future chemical kinetic modelling studies on the pyrolysis and oxidation of 2-methylfuran, or the larger molecular structures for which it is a known pyrolysis/combustion intermediate (*e.g.* cellulose, coals, 2,5-dimethylfuran).

1 Introduction

Dwindling energy reserves, increasing global energy demands and prices, and the threat of irreversible climate change have led to major research efforts focusing on the development of renewable energy sources, which can supplant fossil derived products and meet future demands in an economically, environmentally and socially sustainable manner.

Ethanol is currently the leading biofuel which offers an alternative to gasoline in the transportation sector, with 83.1 billion litres produced in 2012, primarily in Brazil and North America.[1] However, first-generation production methods which compete with food for feedstocks coupled with a low energy density, high vapor pressure, and complete miscibility with water, have led to a re-consideration of its viability as a fossil fuel replacement.[2]

Román-Leshkov and co-workers[3] reported a catalytic strategy for the conversion of fructose to 2,5-dimethylfuran (25DMF) *via* the platform chemical hydroxymethylfurfural (HMF) in 2007, with a host of research since following on processes for the conversion of waste biomass into HMF and in turn furanic based fuels.[4–8]

25DMF has an energy density[3] of 31.5 MJ L^{-1} which is similar to a typical gasoline and a high boiling point, low water solubility, and the ability to use it in current internal combustion engines[9,10]

Combustion Chemistry Centre, National University of Ireland, Galway, Republic of Ireland. E-mail: k.somers1@nuigalway.ie

† Electronic supplementary information (ESI) available: Tabulated pressure- and temperature-dependent rate constants derived from RRKM/ME computations; potential energy surfaces for minor reaction pathways; tabulated electronic energies (0 K and 298.15 K) and geometries for all stationary points; frequencies, rotational constants and other information used in TST/RRKM computations are provided as input files compatible with the Thermo module of the Multiwell program suite; a comparison of high-pressure limiting rate constants reported in the work of Davis and Sarathy[35] with *this work*. The Chemkin-PRO format kinetics, thermochemistry and transport properties files used in the numerical modelling of all experiments; results of computational modelling of literature burning velocities,[32,64] ignition delay times[32,39] and flame speciation measurements.[36] See DOI: 10.1039/c3cp54915a

makes it compatible with current infrastructure. These properties make 25DMF desirable when compared with ethanol, whose lower energy density, boiling point, and greater water solubility prove problematic, although engine tests[9,10] have shown that ethanol performs better than 25DMF in terms of knock resistance and hydrocarbon, nitrous oxide, carbon monoxide and particulate emissions.

Recently 2-methylfuran (2MF) has received similar attention to 25DMF as a possible alternative biofuel, with novel production methods under development.[8] Engine tests have ensued with Thewes *et al.*[11] and Wang *et al.*[12] studying the performance of 2MF in direct-injection spark-ignition engines. Thewes *et al.*[11] found that 2MF has excellent combustion stability, particularly in cold conditions, with hydrocarbon emission reductions of at least 61% compared to a conventional research octane number 95 fuel. Wang *et al.*[12] found that 2MF has a greater thermal efficiency than gasoline and 25DMF, that its overall regulated emissions are comparable with 25DMF, and that its aldehyde emissions are much lower than gasoline and ethanol.

Lifshitz and co-workers studied the decomposition of furan, 2MF and 25DMF[13–15] behind reflected shock waves at temperatures of 1050–1460 K, pressures of 1.5–3.0 atmospheres and residence times of 2 ms. Gas chromatography and mass spectrometry were used to quantify reactant and product species in the post-shock mixtures. A total of 17 products were quantified in their 2MF experiments[14] with CO found to be the major decomposition product. A range of C_1–C_4 species were also quantified along with two oxygenated intermediates, ketene and furan. The order of reactivity of the series of furans was in line with previous studies (25DMF > 2MF > furan).[16,17] The experiments of Lifshitz *et al.*[14] will be discussed in detail in subsequent sections.

The theoretical work by Sendt[18] ultimately rationalised the decomposition pathways of furan, which were originally proposed as being routed through biradical intermediates.[13,16,19] The authors used CASSCF, CASPT2 and G2(MP2) computations to investigate the potential energy surfaces and kinetics of the thermal decomposition of furan. Hydrogen atom migrations on a singlet potential energy surface with the ultimate formation of CO and propyne, and C_2H_2 and ketene, were highlighted as the likely decomposition pathways and a chemical kinetic model constructed by the authors was capable of replicating experimental speciation profiles.[19] They concluded that ring scission of the C–O bond in furan, on either singlet or triplet potential energy surfaces, was simply too endothermic to contribute to the decomposition of the molecule, thus discounting the numerous postulates[13,16,19] of biradical initiated decomposition pathways for furan. Contemporaneously, Liu *et al.*[20,21] reached the same conclusion as Sendt *et al.*

Simmie and Curran[22] used quantum chemical calculations and isodesmic reactions to determine gas-phase formation enthalpies ($\Delta_f H^{\ominus}$) of a range of substituted furans and their radicals at 298.15 K, thus implying bond dissociation energies (BDEs). Their computed $\Delta_f H^{\ominus}$ of -80.8 ± 0.5 kJ mol^{-1} for 2MF is in good agreement with a calorimetric determination[24] of -76.4 ± 1.2 kJ mol^{-1} and subsequent very high-level theoretical determination by Feller and Simmie[23] of -80.3 ± 5 kJ mol^{-1}.

Simmie and Metcalfe[25] used electronic structure calculations to study the potential energy surfaces of a range of unimolecular decomposition, hydrogen atom addition and hydrogen atom abstraction reactions of 25DMF. Transition state theory was used to determine high-pressure limiting rate constants. Abstraction from the alkyl side chain of 25DMF to form the 5-methyl-2-furanylmethyl radical was highlighted as the preferred pathway for metathesis reactions. They also rationalised the formation of 2MF from 25DMF *via* a hydrogen-atom addition methyl-radical elimination sequence.

Quantum chemical calculations by Sirjean and Fournet[29–31] elaborated on the work of Simmie and Metcalfe[25] by further exploration of the potential energy surface for the decomposition reactions of 2,5-dimethylfuran, 5-methyl-2-furanylmethyl radical and the reactions of hydrogen atom with 25DMF. Rice–Ramsperger–Kassel–Marcus theory calculations with master equation analysis was used to determine pressure-dependent rate constants for each system. The decomposition of the 5-methyl-2-furanylmethyl radical was found to result in the formation of cyclohexadienone isomers and a hydrogen atom. Hydrogen atom addition to 25DMF was found to primarily lead to the formation of 2MF and a methyl radical, and to a lesser extent, 1,3-butadiene and acetyl radical. Their computations on the total rate of hydrogen atom termination with 25DMF are in excellent agreement with the shock tube studies of Friese *et al.*[27,28]

Recently, Somers *et al.*[32] described experiments on the oxidation of 2MF, including measurements of ignition delay times and laminar burning velocities, with a chemical kinetic model developed which could adequately replicate these experiments. The model developed by Somers *et al.*[32] was based on preliminary *ab initio* calculations which were not described in detail at the time. The aim of *this work* is to describe those preliminary calculations in a more complete fashion. Quantum-Rice–Ramsperger–Kassel (QRRK) theory with a Modified Strong Collision (MSC) approach, as described by Chang *et al.*,[33] was utilised in the previous work[32] to account for the influence of pressure on reaction rate constants. Here we utilize more rigorous Rice–Ramsperger–Kassel–Marcus (RRKM) theory calculations coupled with an energy grained master equation (ME) solution.

The QRRK/MSC approach varies from the RRKM/ME in two key respects. The first is that the former derives vibrational frequencies for reactants, and subsequent sums and densities of states, from a three-frequency fit to molecular heat capacities.[34] Microscopic rate constants, $k(E)$, are in turn computed from the density of states of the reactant molecule together with an estimate of the high-pressure limiting rate constant for the reaction *via* the Inverse Laplace Transform (ILT) method. No knowledge of the transition state properties is required in this approach, although the high-pressure limiting rate constants can be computed from canonical transition state theory as performed in the work of Somers *et al.*[32] The RRKM method derives sums and densities of states for reactants and transition states, and subsequently $k(E)$, from molecular ro-vibrational data typically obtained from quantum chemical calculations.

The second major difference lies in the approach to collisional energy transfer (CET). Both the MSC and ME approaches assume

that collisions occur based on the Lennard-Jones collision frequency. However, the MSC approximation assumes that every collision is completely activating or de-activating, and the Lennard-Jones collision frequency is simply altered by a weak-collision efficiency factor, β_c, which reduces the total rate of collisions in order to account for the fact that activation and de-activation require many collisions. The ME approach explicitly considers the transfer of energy between different energy levels and is thus a more physically realistic and accurate approximation for CET.

Since the development of the kinetic model by Somers *et al.*[32] a number of noteworthy studies on 2MF oxidation have been carried out contemporaneously with *this work*. Davis and Sarathy[35] reported reaction enthalpies, barrier heights and rate constants for several of the combustion and atmospheric reactions of 2-methylfuran based on quantum chemistry (CBS-QB3, G4) and canonical rate theory. Hydroxyl radical addition to the furan ring and subsequent O_2 addition reactions to the nascent adduct were investigated as possible reactions of significance under atmospheric and low-temperature combustion conditions. They also investigated unimolecular decomposition reactions of 2MF and abstraction reactions by hydrogen atom, although hydrogen atom addition reactions and the influence of pressure on the thermal decomposition pathways rate constants were not investigated. A small number of these high-temperature reactions are described in detail in *this work*, with the high-pressure limiting rate constants determined here in good agreement with the results of Davis and Sarathy.[35] A comparison of our results with Davis and Sarathy is presented in the ESI.†

Tran and co-workers[36] recently studied the flame structure of two laminar premixed low-pressure (20 and 40 mbar) 2MF–O_2–Ar flames, with electron-ionization molecular beam mass spectrometry (EI-MBMS) and GC used to quantify reactant, intermediate and product concentrations as a function of distance from the burner. They provided a chemical mechanism for 2MF oxidation under these conditions, constructed largely by taking analogies to rate constants from 2,5-dimethylfuran[37] and furan[38] mechanisms available in the literature. Their mechanism was shown to satisfactorily reproduce their experimental results, as was the mechanism previously described by Somers *et al.*,[32] although the former was not compared with the ignition delay time or laminar burning velocities against which the latter was also validated. The mechanism developed as part of *this work* is compared with these recently published measurements in the ESI,† with good quantitative predictions of the major species reported experimentally.

Wei *et al.*[39] recently used a shock tube facility to determine ignition delay times of 2MF–O_2–Ar mixtures from equivalence ratios of 0.25–2.0, at temperatures of 1120–1700 K and at pressures of 1.25–10.65 bar. Their measurements are consistent with those of Somers *et al.*[32] at atmospheric pressure and provide valuable new data for kinetic modelling at elevated pressures. The kinetic model of Somers *et al.*[32] was used to numerically model the experimental results with reasonable agreement observed. The updated mechanism described herein is compared with these new ignition measurements in the ESI,† with good reproduction of experimental measurements.

2 Computational methods

Minima and transition states have been initially optimised using the B3LYP[40,41] functional coupled with the 6-31+G(d,p) basis set. Frequency analysis is employed to verify the nature of stationary points with the presence of a single imaginary frequency indicative of a transition structure, which is in turn connected to reactants and products *via* intrinsic reaction coordinate (IRC) calculations.[42]

B3LYP optimised geometries are subject to further geometry optimisation, frequency analysis and single point energy calculations using the compound methods CBS-QB3,[43] CBS-APNO[44] and G3[45] which have been used in numerous theoretical studies for the determination of thermochemistry and kinetics of furanic species.[25,28–31,35,46] The three methods tend to give good agreement with each other, possibly indicating an absence of multi-reference character in the systems studied. Calculations have been carried out using the Gaussian 03 and 09 applications.[47] Where uncertainties in quantum chemical calculations are reported in the text, it is to one standard deviation.

The Thermo application of the Multiwell program suite[48,49] has been used to determine thermochemical parameters (S, C_p and $H_T - H_0$, 298–2500 K) and high-pressure limiting rate constants, from canonical transition state theory. Internal rotations corresponding to low frequency torsional modes are analysed *via* relaxed potential energy surface scans, where geometries and energies are calculated as a function of dihedral angle in 10 degree increments. Potential energy and rotational constants (computed using the LAMM module of Multiwell) as a function of dihedral angle are fit to a series of truncated sine and cosine Fourier series and are used as input for a 1-D internal rotation approximation. For hydrogen atom transfer, abstraction, and addition reactions, the contribution of quantum mechanical tunneling has been accounted for *via* the inclusion of asymmetric Eckart tunneling as implemented in Multiwell.

Standard state enthalpies of formation ($\Delta_f H^\ominus$) of all C_5H_6O species are computed based on the $\Delta_f H^\ominus$ of 2-methylfuran,[23] and $\Delta_r H_0$ (0 K) with subsequent extrapolation *via* enthalpy functions ($H_T - H_0$). $\Delta_f H^\ominus$ of $\dot{C}_5H_7O$ radicals are derived from $\Delta_f H_0$ of 2MF and $\dot{H}$ atom and $\Delta_r H_0$. For the 2-furanylmethyl radical, $\Delta_f H_0$ (78.07 kJ mol^{-1}) is determined from $\Delta_r H_0$ (85.11 kJ mol^{-1}) for the reaction 2MF → $\dot{H}$ + 2-furanylmethyl and the known $\Delta_f H^\ominus$ of 2MF and $\dot{H}$ atom. $\Delta_f H^\ominus$ of all other $\dot{C}_5H_5O$ radicals are computed relative to 2-furanylmethyl radical. Whilst isodesmic reactions could also be employed to determine the above parameters, the lack of well characterized companion species for error cancellation inhibits the development of suitable working reactions, particularly as the acyclic species which are formed upon opening of the 2MF ring are highly functionalised. The above method does ensure a consistent approach to thermochemical computations for inclusion in subsequent kinetic modelling work.

Many of the reactions investigated in *this work* correspond to those which are both temperature- and pressure-dependent. RRKM/ME calculations are used as a framework in order to evaluate the effect of the latter. RRKM/ME analyses of the chemically activated reactions of hydrogen atom with 2MF have been carried out using the stochastic method developed by Barker and co-workers implemented *via* the Multiwell program suite.[48,49] Sums and densities of states of reactants and transition states are evaluated using a direct count method with an energy grain size of 10 cm^{-1}, up to a maximum energy of 10^5 cm^{-1}. In order to minimise stochastic uncertainties for minor reaction pathways, 20×10^6 trials were carried out for 160 collisions at temperatures of 600–2000 K from 1–100 atm; for sub-atmospheric pressures, $1–2 \times 10^6$ trials were employed to minimise computational expense. Ro-vibrationally excited adducts were found to have undergone deactivation within the 160 simulated collisions under these conditions, before thermal unimolecular decay of the intermediate isomers subsequently occurred. Phenomological rate constants for the reaction 2MF + Ḣ → products were determined by monitoring concentration-time and vibrational energy-time profiles of the excited adducts using the Thermal Decay procedure recently described by Pinches and da Silva.[50]

RRKM/ME analyses of the thermally activated unimolecular reactions of 2MF were carried out using the ChemRate code[51] as Multiwell is not optimally designed for the computation of slow steady-state unimolecular reactions where the number of collisions being simulated is greater than a few thousand. In this case, the thermal unimolecular reaction of 2MF is slow below 1750 K and $>10^4$ collisions are required to achieve adequate consumption of the reactant for the extraction of rate constants from concentration-time profiles. For calculations using ChemRate, an energy grain size of 40–70 cm^{-1} was used up to a maximum of 10^5–1.5×10^5 cm^{-1} (depending on the specific temperature being studied). Convergence was monitored by ensuring that solutions to the Master Equation became time-independent with the "Divide and Conquer" method employed. The same method is used for computations on the thermal decomposition of the 2-furanylmethyl radical, although as chemical reaction for this species is much faster than for 2MF, a comparison of pressure-dependent rate constants derived from both Multiwell and ChemRate is presented. All RRKM/ME calculations are carried out based on ro-vibrational and energetic properties from CBS-QB3 calculations.

For all simulations, the average energy transferred in a deactivating collision, $\langle \Delta E_d \rangle$, was assumed to have a temperature-independent value of 1000 cm^{-1}. Many recent literature studies have assumed constant $\langle \Delta E_d \rangle$ values for similar systems (large aromatic molecules). $\langle \Delta E_d \rangle$ estimates have ranged from 2000 cm^{-1} for the benzyl radical,[52,53] 1000 cm^{-1} for a C_7 heterocyclic ring,[55] 718 cm^{-1} for a $C_{10}H_{10}$ biheterocycle,[54] 500 cm^{-1} for pyrazole,[56] fulveneallene[57] and benzyl hydroperoxide,[58] and 260 cm^{-1} for 2,5-dimethylfuran[29–31] and furan.[38] Other recent studies have assumed temperature-dependent energy transfer parameters.[59,60] There is still remaining uncertainty in these energy transfer parameters but our empirical estimate of 1000 cm^{-1} lies well within the range of values adopted in recent literature studies. Some test calculations were carried out with $\langle \Delta E_d \rangle$ = 500 cm^{-1} and $\langle \Delta E_d \rangle$ = 2000 cm^{-1} to illustrate the variation in computed rate constants. The results are found in ESI† and they show less than a factor of 2 variation in the computed rate constants for unimolecular decomposition pathways, and a factor of 2–3 variation in computed rate constants for major chemically activated pathways. All calculations are carried out in an argon bath gas with Lennard-Jones parameters for the third body taken as σ = 3.47 Å and ε/k_B = 114.[61] For 2MF and its derivatives Lennard-Jones parameters were determined empirically from the correlations provided by Kee and co-workers.[62] Together with recommended critical constants for 2MF,[63] σ = 5.36 Å and ε/k_B = 396 are computed. All intermediates from 2MF decomposition, 2-furanylmethyl radical decomposition, and hydrogen atom addition pathways are assumed to have the same Lennard-Jones parameters.

Ultimately, the kinetics and thermochemistry produced as part of *this work* are used as input for a chemical kinetic model to describe the pyrolysis of 2MF, which is then compared with the shock tube data of Lifshitz *et al.*[14] Shock tube simulations were carried out using the Aurora module (constant volume) of the Chemkin-Pro[65] software package with an average residence time of 2.05 ms and an average pressure of 2.5 atm.

3 Results and discussion

In all subsequent sections, the subscript (x) used to enumerate tabulated rate constants (k_x) corresponds with the number assigned to the transition state (**TSx**) for that reaction on a given potential energy surface. If a reaction does not have an accompanying potential energy surface (abstraction reactions or literature rate constants), other shorthand notations are used.

3.1 Carbene mediated unimolecular decomposition

Potential energy surfaces for the formation and decomposition of β-carbenes are depicted in Fig. 1 and 2 with corresponding rate constants (k_5–k_{13}) reported in Table 1. Unimolecular decomposition of 2MF through α-carbene intermediates was found to be uncompetitive with the β-carbene pathways due to due to the higher energy barriers encountered on their potential energy surfaces. A detailed discussion on these pathways can be found in ESI† with the rate constants computed for these pathways (k_1–k_4) reported in Table 1.

A 3 → 2 hydrogen atom transfer, Fig. 1, which forms a β-carbene intermediate (**M4**) has a computed barrier of 294.5 ± 1.6 kJ mol^{-1}. This intermediate could not be located using the CBS-QB3 method (B3LYP/CBSB7 optimisation step), which instead led to the *cis* conformer of 2,3-pentadiene-1-al upon optimisation. The same observation was noted in a computational study for the analogous process in 25DMF.[25]

The CBS-APNO and G3 methods successfully locate this carbene intermediate existing at 256.8 ± 2.9 kJ mol^{-1} above 2MF. The subsequent ring opening reaction of the cyclic carbene is found to be extremely facile, with a transition state (**TS6**) being located 2.8 and 2.5 kJ mol^{-1} *below* the level of the

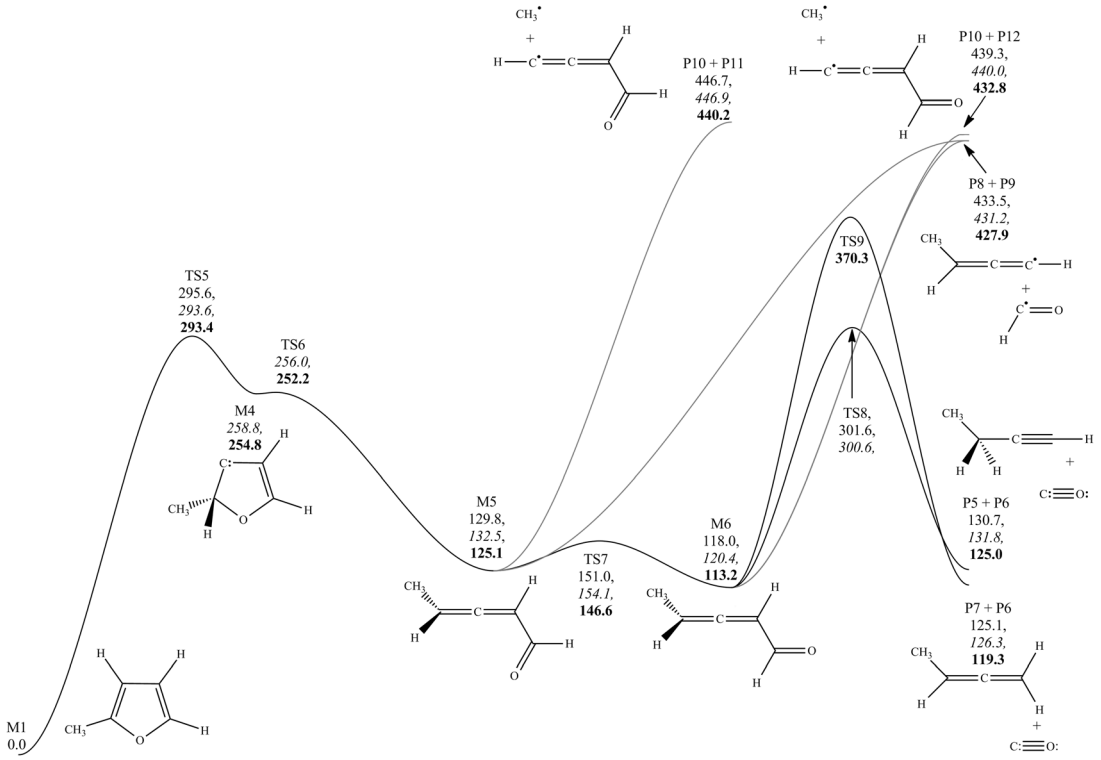

Fig. 1 Potential energy surface for the formation and decomposition of β-carbenes formed from a 3 → 2 hydrogen shift. CBS-QB3, *CBS-APNO* and **G3** energies in kJ mol^{-1} at 0 K relative to 2-methylfuran. Variational processes in greyscale.

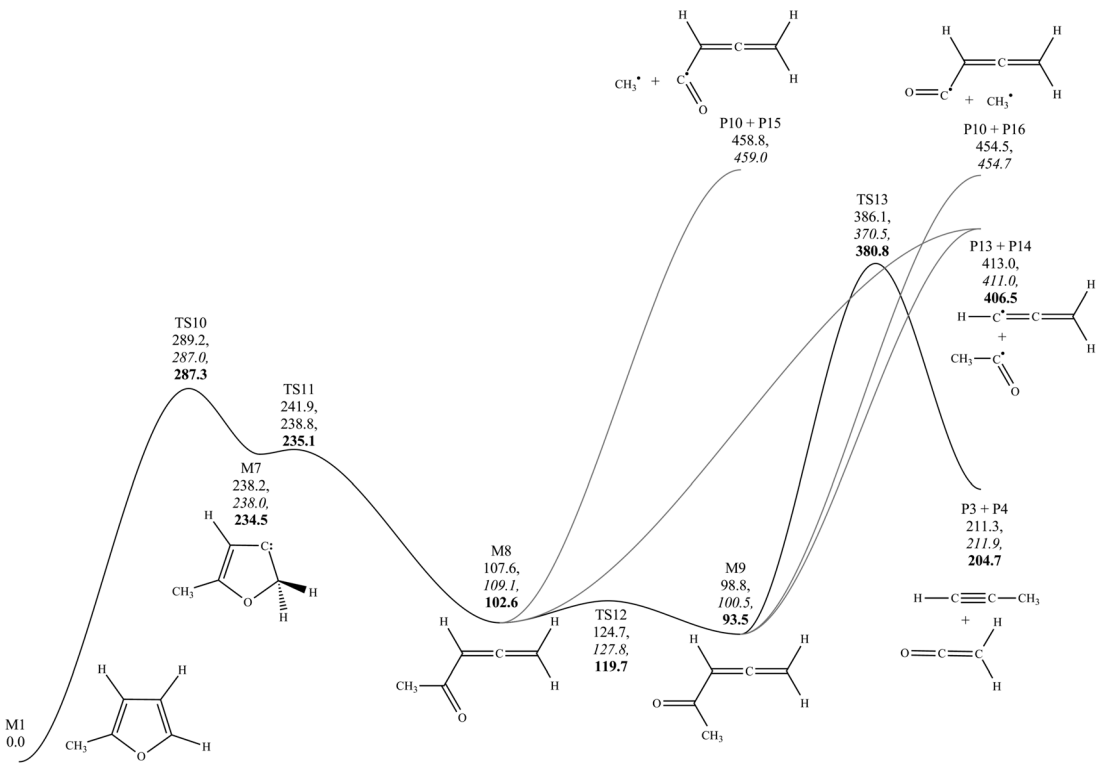

Fig. 2 Potential energy surface for the formation and decomposition of β-carbenes formed from a 4 → 5 hydrogen shift. CBS-QB3, *CBS-APNO* and **G3** energies in kJ mol^{-1} at 0 K relative to 2-methylfuran. Variational processes in greyscale.

Table 1 Arrhenius coefficients of high-pressure limiting rate constants for the decomposition of 2-methylfuran *via* carbene intermediates. $k(s^{-1}) = AT^n \exp(-E_a/R)$, $AT^n(s^{-1})$, E_a/R (K)

No.	Reaction	A	n	E_a/R
k_1	**M1** → **M2**	1.36×10^{11}	0.70	41 593
k_2	**M1** → **M3**	2.26×10^{10}	0.99	32 486
k_3	**M2** → **P1** + **P2**	1.55×10^{12}	0.83	14 343
k_4	**M3** → **P3** + **P4**	8.54×10^{12}	0.68	15 881
k_5	**M1** → **M4**	2.15×10^{10}	0.95	35 145
k_6	**M4** → **M5**	2.80×10^{12}	0.30	−72
k_7	**M5** → **M6**	2.17×10^{13}	−0.24	2725
k_8	**M6** → **P5** + **P6**	7.30×10^{10}	0.69	21 872
k_9	**M6** → **P6** + **P7**	3.40×10^{11}	1.00	30 161
k_{10}	**M1** → **M7**	1.75×10^{10}	1.00	34 174
k_{11}	**M7** → **M8**	6.11×10^{12}	0.09	552
k_{12}	**M8** → **M9**	1.26×10^{13}	−0.13	2146
k_{13}	**M9** → **P3** + **P4**	3.91×10^{08}	1.48	33 817

reactants using the CBS-APNO and G3 methods respectively. The shallow nature of the β-carbene well likely contributes to the inability of the CBS-QB3 method to locate the reactant as a stationary point.

The product of ring opening exists in two rotameric forms (**M5** and **M6**) about the formyl group, which are connected by a rotational barrier of 21.4 ± 0.3 kJ mol^{-1}. The *trans* conformer (**M6**) can undergo CO elimination with a concomitant 1 → 4 hydrogen shift to form 1-butyne (k_8) in a near thermoneutral reaction, with $\Delta_r H_0 = 11.9 \pm 0.7$ kJ mol^{-1}.

The barrier for the process is computed as 183.6 kJ mol^{-1} based CBS-QB3 calculations, and 180.2 kJ mol^{-1} *via* the CBS-APNO method, in good agreement with G2(MP2) calculations[18] (175 kJ mol^{-1}) for the similar process in furan. A 1 → 2 hydrogen atom transfer to form 1,2-butadiene and CO is also possible, although the barrier is much greater at 252.2 kJ mol^{-1}.

Simple fission reactions are also possible for this acyclic species and BDEs of C–C bonds in the system have therefore been investigated, as they should coincide effectively with the barrier for these dissociation reactions. The formation of formyl radical (HĊO) and 1,2-butadiene-1-yl radical (ĊH═C═CH–CH$_3$) from the *trans* conformer is found to be endothermic by 321.7 kJ mol^{-1} based on standard state CBS-QB3 energetics, with fission to form a ĊH$_3$ radical and a formyl allene radical (ĊH═C═CH–CH═2O) having a similar BDE of 327.9 kJ mol^{-1}. These homolytic processes face enthalpic barriers much greater than that computed for the lowest energy CO elimination process (circa 140 kJ mol^{-1}), and are therefore unlikely to contribute to the decomposition of the aldehyde.

β-Carbene formation (**M7**) *via* a 4 → 5 hydrogen shift (Fig. 2) proceeds through a barrier of 287.8 ± 1.2 kJ mol^{-1}, similar to that observed for the 2 → 3 hydrogen shift. The carbene can undergo ring opening through **TS11**, in an effectively barrierless process (1.69 ± 1.7 kJ mol^{-1}) to form 3,4-pentadiene-2-one.

Like the formyl butadiene product formed from a 3 → 2 hydrogen atom transfer, there exists *cis* and *trans* conformers of 3,4-pentadiene-2-one (**M8** and **M9**) with the *trans* conformer (**M9**) capable of undergoing a 1 → 5 hydrogen shift in a concerted process to form ketene and propyne. A barrier of 287.3 kJ mol^{-1} is computed at the CBS-QB3 level of theory.

Given the tight nature of the transition state, we calculate a decrease in $\Delta^{\ddagger}S$ of −3.3 kJ mol^{-1} at standard temperature and only a slight increase in $\Delta^{\ddagger}S$ to 1.0 kJ mol^{-1} at 2000 K. C–C bond fission of the more stable *trans* conformer to acetyl radical (CH$_3$–Ċ═O) and the propargyl radical (CH≡C–ĊH$_2$) is computed to be endothermic by 317.7 ± 1.8 kJ mol^{-1}, with the formation of a ĊH$_3$ radical and a formyl allene radical (CH$_2$═C═CH–Ċ═O) found to be endothermic by 359.1 ± 4.5 kJ mol^{-1}.

The formation of CH$_3$–Ċ═O and CH≡C–ĊH$_2$ radicals is energetically similar to the concerted elimination process and we therefore expect that simple fission is likely to be favoured over the elimination reaction at high temperatures, as the looser nature of the homolysis reaction is likely to result in an increase in $\Delta^{\ddagger}S$ for the reaction.

Fig. 3, and Tables 1 and 2, show calculated rate constants for the formation of carbenes in the homologous series furan, 2MF and 25DMF, with consistent rate constants emerging for the formation of α- and β-carbenes *via* hydrogen atom and methyl group shifts.

Comparison is made with the computations of Simmie and Metcalfe[25] for the 25DMF system and Sendt *et al.*[18] who reported Arrhenius parameters for this process in furan. Rate constants

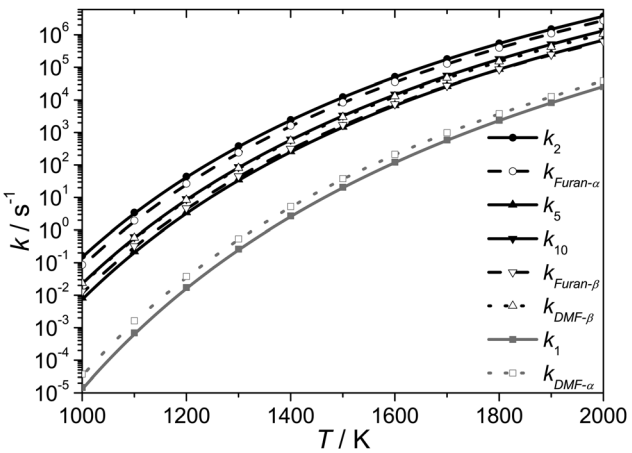

Fig. 3 A comparison of the high-pressure limiting rate constants for –H (black) and –CH$_3$ (grey) group transfer reactions in the homologous series furan (– –), 2-methylfuran (—) and 2,5-dimethylfuran (···). Furan and 2,5-dimethylfuran rate constants are reduced by a factor of two to account for the external symmetry number of 1 for 2-methylfuran.

Table 2 Arrhenius coefficients of high-pressure limiting rate constants for –H and –CH$_3$ group shifts in 2,5-dimethylfuran and furan. $k(s^{-1}) = AT^n \exp(-E_a/R)$, $AT^n(s^{-1})$, E_a/R (K)

No.	Reactant	Carbene, –R	A	n	E_a/R
$k_{\text{Furan-}\alpha}$	Furan[a]	α, –H	1.69×10^{12}	0.56	33 782
$k_{\text{Furan-}\beta}$	Furan[b]	β, –H	5.94×10^{13}	0.00	35 372
$k_{\text{DMF-}\alpha}$	25DMF[c]	α, –CH$_3$	7.77×10^{13}	0.00	41 483
$k_{\text{DMF-}\beta}$	25DMF[c]	β, –H	9.48×10^{13}	0.00	35 230

[a] *This work.* [b] Sendt *et al.*[18] [c] Simmie and Metcalfe.[25]

for furan and 25DMF decomposition are reduced by a factor of two in Fig. 3 for comparison with 2MF, given the loss of symmetry for the mono-alkylated furan, but those reported in Table 2 have not undergone this treatment. There is a close agreement within the computed rate constants amongst the homologous series, which may be of interest to kinetic modellers.

RRKM/ME analysis has been applied to determine pressure- and temperature-dependent rate constants for the multi-step collisionally activated decomposition pathways of 2MF. A number of simplifications are made to the potential energy surface for decomposition through β-carbenes. Both **M4** and **M7** are omitted from the RRKM/ME calculations as preliminary calculations showed that collisional stabilisation is inefficient for these species, owing to their shallow well-depth. Only a single rotamer of 2,3-pentadiene-1-al (**M6**) and of 3,4-pentadiene-2-one (**M9**) is included in this analysis for simplicity.

Pressure-dependent rate constants for the β-carbene mediated decomposition of 2-methylfuran are shown in Fig. 4. Under the experimental conditions of Lifshitz *et al.* (1150–1500 K, 2.5 atm), both reaction pathways are approximately at the high-pressure limit, with only ≈20% reduction in the computed high-pressure limiting rate constants at 1500 K and 2.5 atm. With increasing temperature and decreasing pressure however, the deviation of the rate constants from the high-pressure limiting case becomes more pronounced and there may be a need to account for fall-off effects under these conditions.

As part of our RRKM/ME calculations, we also consider the simple fission of 2MF into 2-furanylmethyl radical and Ḣ atom. The high-pressure limiting rate constant for this barrierless process is estimated based on an analogy with a literature[66] rate constant for the recombination of a Ḣ atom with the resonantly stabilised benzyl radical. From an estimated recombination rate constant of $9.25 \times 10^{13}\,T^{-0.01}\exp(-96.9/T)$ cm^3 mol^{-1} s^{-1} and the equilibrium constant for the reaction 2-furanylmethyl + Ḣ atom ⇋ 2MF, a high-pressure limiting rate constant of $3.37 \times 10^{15}\,T^{-0.01}\exp(-44\,026/T)$ s^{-1} for the dissociation reaction is computed through microscopic reversibility.

For the alkyl side chains of 2MF[22] and toluene[67] similar BDEs have previously been reported, 360.9 ± 5.2 and 375 ± 5.0 kJ mol^{-1} respectively. A BDE of 361.2 kJ mol^{-1} for 2MF is determined in *this work*. The high-pressure limiting rate constant of the barrierless association of a Ḣ atom with the 2-furanylmethyl radical may be expected to be of a similar order as that for the recombination of Ḣ atom with benzyl radical, and the high-pressure limiting rate constant described above should therefore be of a reasonable order.

Transition state properties (frequencies, rotational constants) for the C–H fission process have been generated automatically by the ChemRate code based on the properties of the reactants and products for the reaction and the microscopic rate constants, $k(E)$, were then determined from the estimated transition state properties. $k(E)$ were subsequently altered by an empirical fitting factor such that the high-pressure limiting rate constant described above was replicated at every temperature. The enthalpy of activation for the process was assumed equal to the the enthalpy of reaction at 0 K.

Based on temperature- and pressure-dependent RRKM/ME calculations under the conditions of Lifshitz *et al.* study,[14] as shown in Fig. 5(a), decomposition *via* β-carbene intermediates is found to be dominant over the temperature range 1000–2000 K. 3 → 2 and 4 → 5 hydrogen atom shift reactions forming **M6** and **M9** are preferred to the simple fission of a C–H bond, and the formation of $CH_2{=}C{=}O$ and $CH{\equiv}C{-}CH$ through an α-carbene (**M3**).

Whilst a hydrogen atom transfer reaction to form an α-carbene (**M3**) is initially competitive with β-carbene formation (Fig. 3), unlike the β-carbenes which can readily undergo ring opening, the α-carbene faces subsequent and much more substantial barriers in order to decompose to bimolecular products. A steady state analysis is employed at each pressure to compute

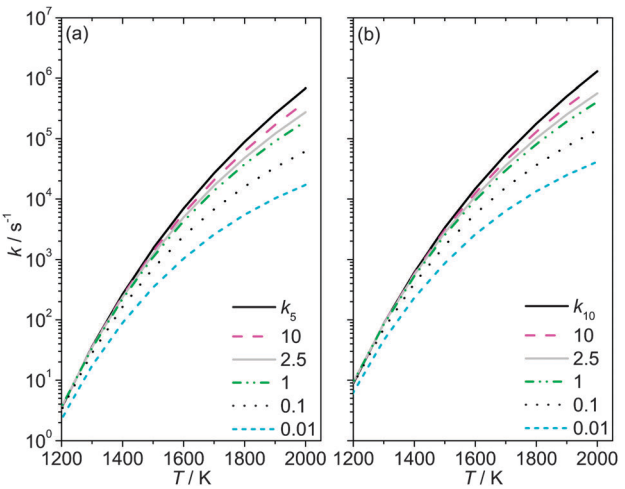

Fig. 4 Computed pressure-dependent rate constants (atm) for the decomposition of 2-methylfuran to (a) 2,3-pentadiene-1-al (**M6**) and (b) 3,4-pentadiene-2-one (**M9**).

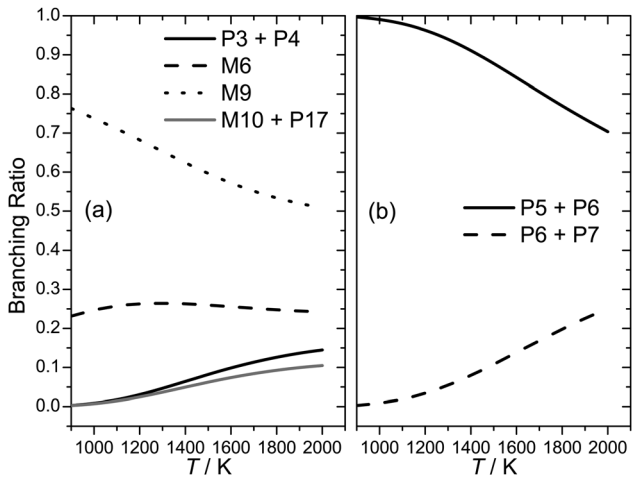

Fig. 5 Temperature-dependent branching ratios for the thermal decomposition of 2-methylfuran under the conditions of the Lifshitz *et al.*[14] study (2.5 atm). (a) 2-Methylfuran → products; **P3** + **P4** (ketene + propyne *via* α-carbene), **M6** (2,3-pentadiene-1-al *via* β-carbene), **M9** (3,4-pentadiene-2-one *via* β-carbene), **M10** + **P17** (C–H fission) (b) **M6** → products; **P5** + **P6** (1-butyne + CO), **P6** + **P7** (1,2-butadiene + CO).

the fraction of 2MF which will form $CH_2{=}C{=}O$ and $CH{\equiv}C{-}CH$ *via* **M3** and the results show that only above 1500 K and pressures of 1 atm will this pathway become competitive. C–H fission is found to be the least important unimolecular decomposition pathway of 2MF based on the present analysis.

The temperature-dependent branching ratios for the decomposition of **M6** are shown in Fig. 5(b). **M6** can decompose to form 1-butyne and CO or 1,2-butadiene and CO, with the former being favoured over the entire temperature and pressure range of Lifshitz *et al.* study.[14] The latter becomes competitive only at higher temperatures. **M9** is found to decompose exclusively to $CH_3{-}\dot{C}{=}O$ and $CH{\equiv}C{-}\dot{C}H_2$ radicals under all conditions of temperature and pressure. The high-pressure limiting rate constant for this reaction has been estimated in a similar fashion to the C–H fission reaction of 2MF, with an assumed rate constant for the recombination of $CH_3{-}\dot{C}{=}O$ and $\dot{C}H_2{-}C{\equiv}CH$ radicals of $5.2 \times 10^{12} T^{0.01} \exp(-114/T)$ cm^3 mol^{-1} s^{-1}. This implies a forward decomposition rate constant of $1.52 \times 10^{25} T^{-2.48} \exp(-39\,621/T)$ s^{-1}, which is ≈200 times faster than the tighter process (k_{13}) forming ketene and propyne.

In conclusion, the unimolecular decomposition of 2-methylfuran is shown to be initiated by 3 → 2 and 4 → 5 hydrogen atom shift reactions which are quite close to their high-pressure limits under the experimental conditions of Lifshitz *et al.*[14] Once sufficient free radical species are formed from the initial decomposition processes, abstraction of a hydrogen atom from the alkyl side chain should assume importance in the pyrolysis of this species. The unimolecular decomposition of 1-butyne and acetyl radical, which are formed as fragmentation products of 2MF, should result in the formation of methyl radicals, with the formation of hydrogen atoms from simple fission also possible but of lesser importance initially. Rate constants for abstraction processes by these radicals are therefore of interest, as is the fate of the primary fuel radical.

3.2 Abstraction reactions and thermal decomposition of 2-furanylmethyl radical

Results of thermochemical and kinetic computations on hydrogen atom abstraction reactions by Ḣ atom and $\dot{C}H_3$ radical are listed in Table 3.

Abstraction of a hydrogen atom from the methyl group of 2MF by a $\dot{C}H_3$ radical is calculated to be exothermic by −74.9 ± 4.0 kJ mol^{-1}, with a barrier of 39.3 ± 4.0 kJ mol^{-1}. Abstraction from the same site by a Ḣ atom faces lower barriers (27.9 ± 2.8 kJ mol^{-1}) but the exothermicity (−77.7 ± 2.8 kJ mol^{-1}) is of a similar order to that for abstraction by a $\dot{C}H_3$ radical.

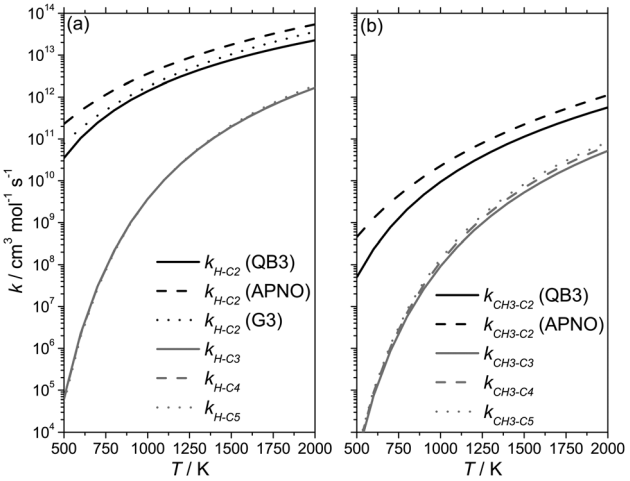

Fig. 6 Rate constants for hydrogen atom abstraction from 2-methylfuran by (a) hydrogen atom and (b) methyl radical. k_{H-C_3}, k_{H-C_4} and k_{H-C_5} are effectively superimposed.

Abstraction of any of the hydrogen atoms directly bonded to the furan ring is thought to be unlikely given their highly vinylic nature, with BDEs circa 505 kJ mol^{-1} reported previously.[22] Consistent rate constants for hydrogen atom abstraction by a $\dot{C}H_3$ radical and a Ḣ atom are reported for abstraction from these sites but it is evident that these processes are of little importance, Fig. 6. As a result, the consumption reactions of the furyl radicals formed from these abstraction processes are not considered here.

Rate constants for abstraction from the alkyl group by a Ḣ atom, k_{H-C_2}, are reported in Table 3 at three levels of theory, thus allowing for an assessment of the uncertainty in the computed rate constants. A factor of 2.5 variation is computed at temperatures of 1000–2000 K. In the same range of T, abstraction by methyl radical ($k_{CH_3-C_2}$) varies by a similar order.

The fate of the primary radical (**M10**) formed from abstraction from the alkyl side chain is depicted in Fig. 7 with corresponding rate constant computations given in Table 4. Lifshitz included

Table 3 Computed barrier heights and enthalpies of reaction (kJ mol^{-1}, 0 K) and Arrhenius coefficients of high-pressure limiting rate constants for the reaction 2-methylfuran + Ẋ → Ṙ + XH. k(cm^3 mol^{-1} s^{-1}) = $AT^n \exp(-E_a/R)$, AT^n(cm^3 mol^{-1} s^{-1}), E_a/R (K)

No.	Ẋ	Site	$\Delta^{\ddagger}H_0$	$\Delta_r H_0$	A	n	E_a/R
k_{H-C_2} (QB3)	Ḣ	C-2	26.6	−80.9	5.36×10^4	2.73	1785
k_{H-C_2} (APNO)	Ḣ		25.9	−76.4	8.71×10^0	3.88	57
k_{H-C_2} (G3)	Ḣ		31.1 ± 2.8	−75.7 ± 2.8	5.51×10^{-1}	4.20	216
k_{H-C_3}	Ḣ	C-3	85.1 ± 3.4	64.1 ± 3.3	1.53×10^8	1.86	9666
k_{H-C_4}	Ḣ	C-4	84.2 ± 3.3	63.4 ± 3.1	1.37×10^8	1.88	9700
k_{H-C_5}	Ḣ	C-5	87.3 ± 3.7	63.4 ± 3.8	1.03×10^8	1.94	9838
$k_{CH_3-C_2}$ (QB3)	$\dot{C}H_3$	C-2	40.0	−78.1	1.21×10^{-2}	4.29	2254
$k_{CH_3-C_2}$ (APNO)	$\dot{C}H_3$		38.6 ± 1.0	−76.2 ± 4.0	4.36×10^{-7}	5.58	50
$k_{CH_3-C_3}$	$\dot{C}H_3$	C-3	82.0 ± 0.3	66.9 ± 4.5	1.04×10^2	3.18	8274
$k_{CH_3-C_4}$	$\dot{C}H_3$	C-4	82.5 ± 0.4	66.2 ± 4.3	1.31×10^2	3.19	8336
$k_{CH_3-C_5}$	$\dot{C}H_3$	C-5	82.9 ± 0.8	66.2 ± 5.1	1.54×10^2	3.20	8397

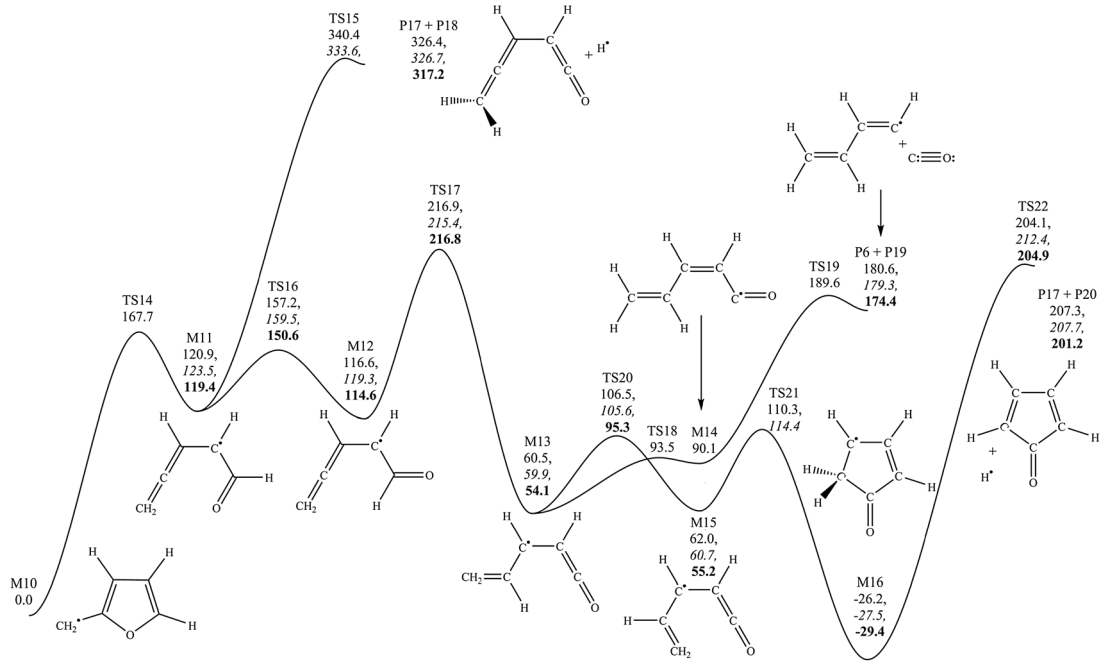

Fig. 7 Potential energy surface for the decomposition of the 2-furanylmethyl radical. CBS-QB3, *CBS-APNO* and **G3** energies in kJ mol^{-1} at 0 K relative to 2-furanylmethyl.

Table 4 Arrhenius coefficients of high-pressure limiting rate constants for the decomposition of 2-furanylmethyl radical (**M10**) and related intermediates. $k(s^{-1}) = AT^n \exp(-E_a/R)$, $AT^n(s^{-1})$, E_a/R (K)

No.	Reaction	A	n	E_a/R
k_{14}	**M10** → **M11**	1.38×10^{13}	0.30	20 480
k_{15}	**M11** → **P17** + **P18**	9.12×10^{10}	1.15	26 634
k_{16}	**M11** → **M12**	4.01×10^{13}	−0.08	4541
k_{17}	**M12** → **M13**	9.54×10^{06}	1.62	10 071
k_{18}	**M13** → **M14**	1.50×10^{13}	−0.19	4046
k_{19}	**M14** → **P6** + **P19**	8.61×10^{14}	0.19	12 822
k_{20}	**M13** → **M15**	2.31×10^{13}	−0.13	5663
k_{21}	**M15** → **M16**	4.06×10^{12}	−0.15	5622
k_{22}	**M16** → **P17** + **P20**	2.99×10^{11}	1.14	28 149
k_{23a}	**P20** → **INT1**	1.03×10^{10}	1.21	36 232
k_{23b}	**INT1** → **P18**	8.72×10^{12}	0.21	2987

decomposition reactions for this radical in their proposed kinetic scheme with the formation of CO and the internal butadienyl radical ($CH_2{=}\dot{C}{-}CH{=}CH_2$) proposed as the major decomposition product. Decomposition to HĊO radical and vinylacetylene ($HC{\equiv}C{-}CH{=}CH_2$), ketene and propyne, or $CH{\equiv}CH$, $\dot{C}_2H_3$ radical and CO was also included in their scheme, although no mechanistic proposals were made. In the temperature range 1100–1600 K, a total decomposition rate constant of $3.81 \times 10^{15} T^{0.11} \exp(-32\,149/T)$ s^{-1} is inferred from their work.

Ring opening of **M10** proceeds *via* cleavage of the C–O bond through a barrier of 167.9 kJ mol^{-1} from CBS-QB3 calculations with both CBS-APNO and G3 failing to locate the transition structure **TS14**. A high-pressure limiting rate constant of $1.38 \times 10^{13} T^{0.3} \exp(-20\,480/T)$ s^{-1} is calculated for the ring opening process from CBS-QB3 calculations.

The ring opening product, 3,4-pentadiene-1-one-2-yl radical, has multiple conformers but only two are of interest mechanistically, **M11** and **M12**. The latter conformer can undergo a 1 → 4 intramolecular hydrogen abstraction reaction through a five membered ring transition state (**TS17**), in a relatively low barrier (99.5 ± 3.1 kJ mol^{-1}) exothermic (−58.7 ± 2.3 kJ mol^{-1}) process. Reformation of **M12** from **M13** is unlikely due to the exothermicity of the reaction, and subsequent low energy exit channels which exist for the consumption of **M13**.

The β-scission of a C–H bond in **M11** to form 1,3,4-pentatriene-1-one (**P18**) was investigated as this species was detected experimentally in the flames of 25DMF[26] and 2MF.[69] With an endothermicity of 202.2 ± 3.9 kJ mol^{-1} and critical energy of 218.4 ± 1.5 kJ mol^{-1}, its formation is not competitive with the 1 → 4 intramolecular hydrogen abstraction reaction.

The product of the 1 → 4 hydrogen atom transfer reaction has two resonance structures that lead to different configurational isomers, **M13** and **M14**, connected by a transition state which lies 33.1 kJ mol^{-1} above **M13** and 3.4 kJ mol^{-1} above **M14**. IRC analysis (B3LYP/CBSB7) verifies the latter isomer undergoes decarbonylation (**TS19**) to form *n*-butadienyl radical ($\dot{C}H{=}CH{-}CH{=}CH_2$) and CO through a barrier of 99.4 kJ mol^{-1}. **M15**, a second conformer of **M13**, can undergo ring closure *via* a barrier of 51.0 ± 3.9 kJ mol^{-1} (**TS21**) to form a resonantly stabilised cyclopentenone radical (**M16**) which is is computed to be 27.7 ± 1.6 kJ mol^{-1} more stable than the 2-furanylmethyl radical.

The β-scission of a C–H bond is the only plausible consumption channel envisaged for (**M16**), forming cyclopentadienone (**P20**) and a hydrogen atom. The barrier for the endothermic process (233.1 ± 4.8 kJ mol^{-1}) is calculated to be 234.8 ± 4.8 kJ mol^{-1}, although the CBS-QB3 method predicts a negative critical

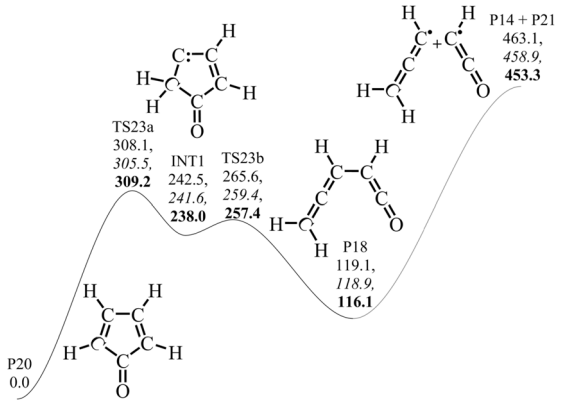

Fig. 8 Carbene intermediate in the isomerisation of 2,4-cyclopendadienone and 1,3,4-pentatrieneone. CBS-QB3, *CBS-APNO* and **G3** energies in kJ mol^{-1} at 0 K relative to reactant.

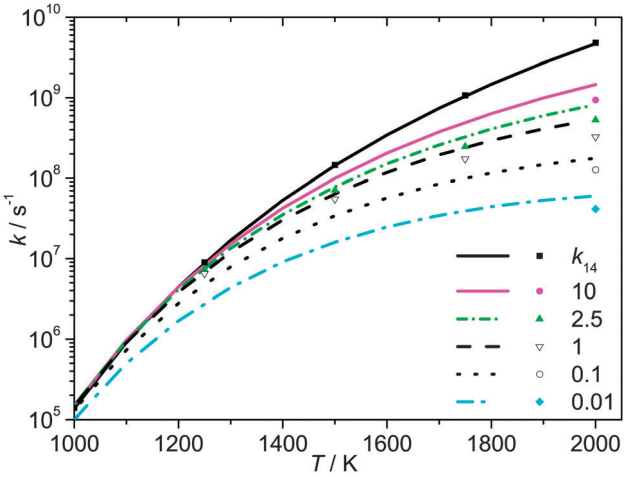

Fig. 9 Pressure- (atm) and temperature-dependent rate constants for the thermal decomposition of 2-furanylmethyl (**M10**) based on RRKM/ME calculations. ChemRate (—), Multiwell (symbols).

energy (−3.19 kJ mol^{-1}) if viewed from the perspective of hydrogen atom addition across the double bond of cyclopentadienone.

Cyclopentadienone is a known intermediate in the combustion of cyclopentadiene and it is interesting to see a common feature between this five-membered ring and 2MF, namely, the formation and consumption of β-carbenes through a 1 → 2 hydrogen shift reaction on a singlet potential energy surface, Fig. 8. The energetics and kinetics of the process were not considered in a previous analysis of cyclopentadienone decomposition.[68] Here we find they are of a similar order to those found in the decomposition of 2MF, with the computed rate constant for the hydrogen transfer reaction (k_{23a}) within a factor of two of those calculated for 2MF (k_5 and k_{10}) in the high-temperature regime. The carbene intermediate (**INT1**) can undergo ring-opening to form 1,3,4-pentatriene-1-one, which was detected in low-pressure flames of 25DMF[26] and 2MF.[69]

The formation of CO and *n*-butadienyl radical appears dominant in our scheme, once **M13** is formed the rate limiting steps for the formation of products are given by k_{19} and k_{22}, with k_{19} dominant in the temperature ranges we have studied.

Multiple-well, multiple-channel RRKM/ME calculations have been carried out to study the influence of pressure on the consumption of all $\dot{C}_5H_5O$ isomers. As a test of the uncertainty in the computed rate constants, both the Multiwell and ChemRate codes were employed in this analysis, with 10^6 trials used in the former. The computed rate constants for the thermal decomposition of **M10** (Fig. 9) are within 30% of each other under all conditions studied. For all other intermediates, a factor of two difference was observed in the worst case scenario for the reaction **M15** → **M16** at 0.01 atm and 2000 K. The computed rate constants from the two codes are therefore in excellent agreement and a comparison of computed rate constants is presented in the ESI.† The fall-off in the rate constant k_{14} appears to be non-negligible under high-temperature, low-pressure conditions and this fall-off effect must be considered in kinetic modelling studies, for example the low-pressure flames of Tran and co-workers[36] and Wei *et al.*[69] Rate constants computed using the ChemRate code from 0.01–100 atm and 800–2000 K are provided in the ESI† for all reactions on the $\dot{C}_5H_5O$ potential energy surface, and are incorporated into our kinetic model as pressure-dependent reactions (Chemkin-Pro PLOG format).

3.3 Hydrogen atom addition reactions

Computed barrier heights, enthalpies of reaction and rate constants for Ḣ atom addition to 2MF are presented in Table 5 and Fig. 10. Consistent reaction barriers and enthalpies of reaction are calculated for these processes. Ḣ atom addition to carbons adjacent to the oxygen atom of the furan ring are much more exothermic (≈45 kJ mol^{-1}) than addition to C-3/C-4, and are thus favoured in terms of computed barriers heights. The difference in the computed Δ_rH_0 upon addition at C-2 and C-5 *versus* C-3 or C-4 stems from the ability of the radicals to delocalise their unpaired electrons within the furan ring, with addition at sites removed from the oxygen atom resulting in

Table 5 Computed barrier heights and enthalpies of reaction (kJ mol^{-1}, 0 K), and Arrhenius coefficients of high-pressure limiting rate constants for hydrogen atom addition reactions to 2-methylfuran. k(cm^3 mol^{-1} s^{-1}) = $AT^n \exp(-E_a/R)$, AT^n(cm^3 mol^{-1} s^{-1}), E_a/R (K)

No.	Site	$\Delta^{\ddagger}H_0$	Δ_rH_0	A	n	E_a/R
k_{24} (QB3)	C-2	12.2	−126.5	2.10×10^8	1.57	904
k_{24} (APNO)		12.9	−128.0	2.67×10^7	1.89	776
k_{24} (G3)		9.5	−127.3	3.33×10^7	1.88	421
		11.5 ± 1.8	−127.3 ± 0.8			
k_{40} (QB3)	C-3	17.5	−80.9	3.72×10^8	1.54	1414
k_{40} (APNO)		18.9	−82.4	3.48×10^7	1.87	1282
k_{40} (G3)		18.7	−80.7	3.94×10^7	1.86	1281
		18.4 ± 0.8	−81.3 ± 0.9			
k_{53} (QB3)	C-4	19.9	−84.6	2.01×10^8	1.61	1672
k_{53} (APNO)		20.7	−85.9	1.88×10^7	1.95	1500
k_{53} (G3)		20.1	−85.3	2.10×10^7	1.94	1460
		20.2 ± 0.4	−85.3 ± 0.7			
k_{60} (QB3)	C-5	7.0	−133.2	1.20×10^9	1.48	468
k_{60} (APNO)		9.6	−133.9	9.06×10^7	1.80	457
k_{60} (G3)		6.2	−132.3	1.30×10^8	1.76	127
		7.6 ± 1.8	−133.1 ± 0.8			

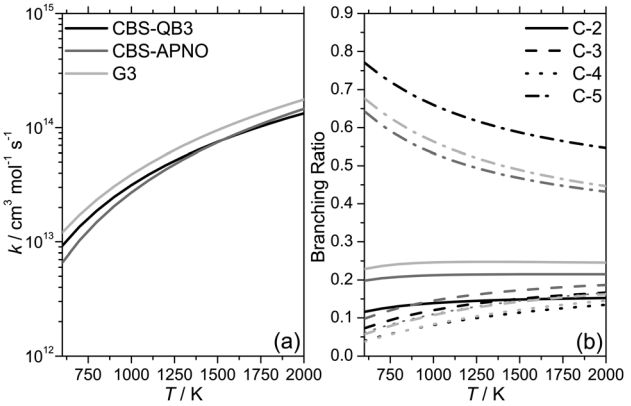

Fig. 10 (a) Total high-pressure limiting rate constant for hydrogen atom addition to 2-methylfuran and (b) site-specific branching ratios at various levels of theory. Colour scheme for theoretical methods in (a) also applies to (b).

radicals incapable of doing so. Rate constants are presented at three levels of theory for an assessment of their uncertainty. The total rate constant for hydrogen atom addition to 2MF varies by less than a factor of two across the three levels of theory applied, with site-specific branching ratios also predicting the following trend quite consistently amongst the methods: C-5 > C-2 > C-3 = C-4. This trend is in line with the reaction exothermicity upon addition at each site.

3.3.1 Addition at C-2. The potential energy surface for hydrogen atom addition to C-2 of 2MF is illustrated in Fig. 11 and 12 with the corresponding rate constants provided in Table 6. The fate of the adduct formed from hydrogen atom addition at C-2 (**M17**) was previously investigated by Simmie and Metcalfe.[25] The authors calculated a rate constant of $2.232 \times 10^{14} \exp(-16\,292/T)$ s^{-1} for the demethylation process forming furan and a $\dot{C}H_3$ radical *via* **TS24**.

However, the authors did not investigate the result of cleavage of the C–O bond which could open the furan ring. Two chiral transition states were identified for this process (**TS26** and **TS30**) which are verified by IRC analysis to form *Z*- and *E*-conformers (**M18** and **M21**) of 3-pentene-1-one-2-yl radical. A total rate constant for ring opening can be determined from the summation of k_{26} and k_{30}. A rate constant of $8.69 \times 10^{12}\, T^{0.16} \exp(-11\,042/T)$ s^{-1} is thus computed, indicating that ring opening should be competitive with demethylation throughout the temperature range 1000–2000 K.

Both **M19** and **M22** can undergo a 1 → 4 hydrogen atom shift reaction to form an aldehydic radical (**M20**) which can decarbonylate through **TS29** in a reasonably low barrier process (101.9 kJ mol^{-1}) forming 1-butene-1-yl radical and CO. Mechanistically, this process is similar to that observed in the decomposition of the 2-furanylmethyl radical, where an aldehydic-type radical is formed before subsequent α-scission to form CO and *n*-butadienyl radical.

Further reactions of **M18** which could lead to the formation of either 1,3-butadiene and HĊO radical or cyclopentadiene and ȮH radical were also investigated, Fig. 12. The formation of 1,3-butadiene and HĊO radical is inhibited firstly by a 1 → 4 hydrogen atom transfer from **M23** to form **M24** *via* **TS34**, for

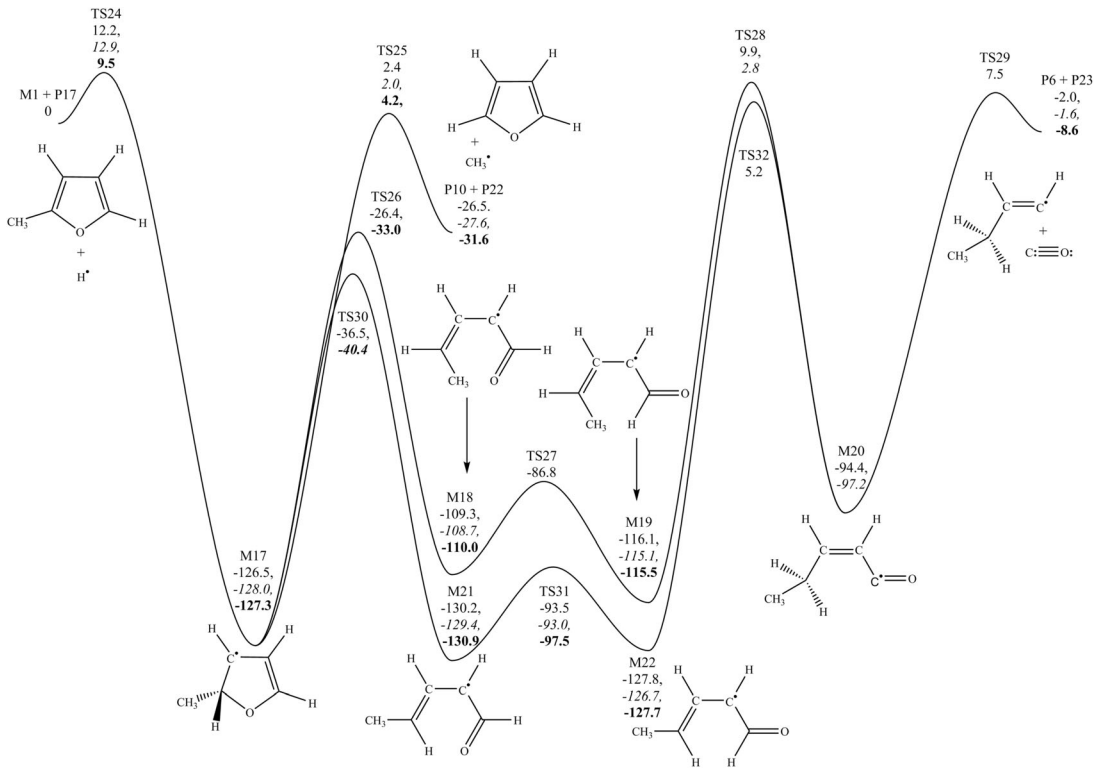

Fig. 11 Potential energy surface for hydrogen atom addition at carbon 2 of 2-methylfuran. CBS-QB3, *CBS-APNO* and **G3** energies in kJ mol^{-1} at 0 K relative to reactants.

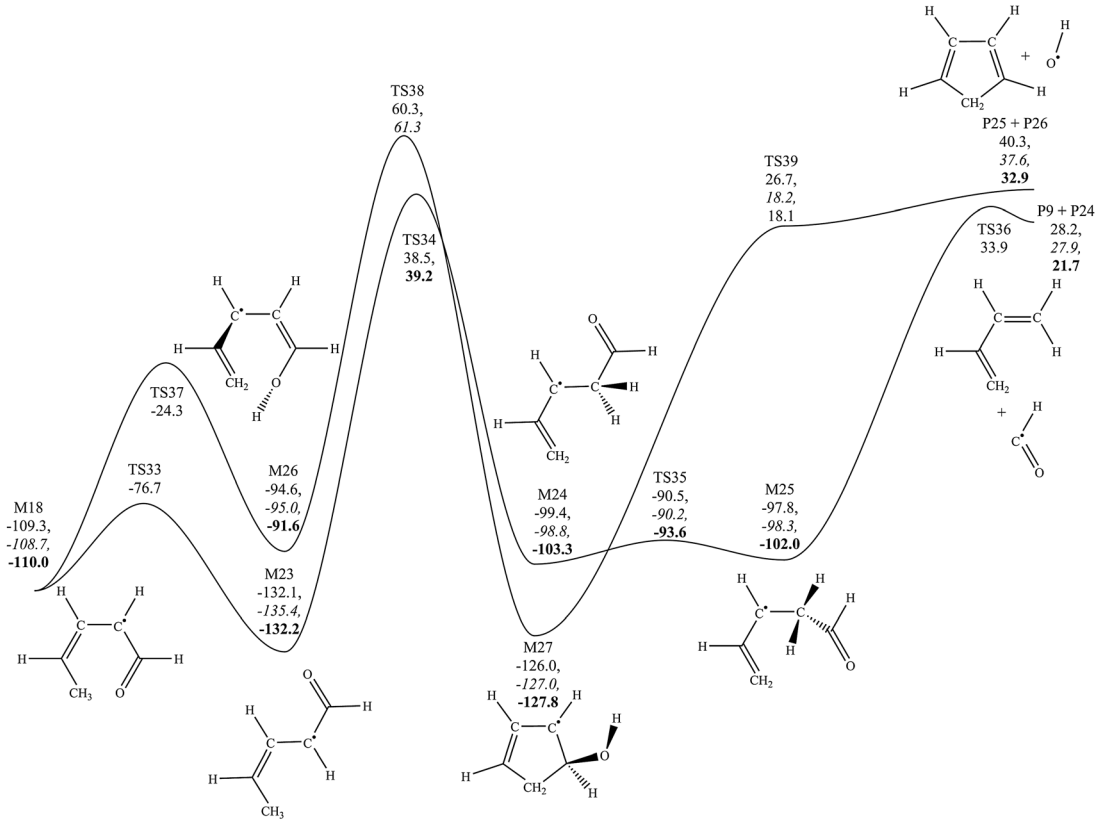

Fig. 12 Potential energy surface for hydrogen atom transfer reactions of 3-pentene-1-al-3-yl radical. CBS-QB3, *CBS-APNO* and **G3** energies in kJ mol^{-1} at 0 K relative to 2-methylfuran and hydrogen.

Table 6 Arrhenius coefficients of high-pressure limiting rate constants for for reactions relevant to hydrogen atom addition at C-2 of 2-methylfuran. $k(s^{-1}) = AT^n \exp(-E_a/R)$, $AT^n(s^{-1})$, E_a/R (K)

No.	Reaction	A	n	E_a/R
k_{25}	**M17** → **P10** + **P22**	9.23×10^{12}	0.38	15 837
k_{26}	**M17** → **M18**	3.85×10^{13}	−0.09	12 216
k_{27}	**M18** → **M19**	2.61×10^{11}	0.58	2710
k_{28}	**M19** → **M20**	2.49×10^{03}	2.59	12 236
k_{29}	**M20** → **P6** + **P23**	1.19×10^{15}	0.26	13 053
k_{30}	**M17** → **M21**	3.85×10^{13}	−0.09	11 003
k_{31}	**M21** → **M22**	2.33×10^{12}	0.26	4422
k_{32}	**M22** → **M20**	3.77×10^{05}	2.03	13 440
k_{33}	**M18** → **M23**	9.21×10^{10}	0.53	3834
k_{34}	**M23** → **M24**	1.83×10^{08}	1.41	19 235
k_{35}	**M24** → **M25**	2.18×10^{10}	0.50	746
k_{36}	**M25** → **P9** + **P24**	2.67×10^{10}	1.20	15 994
k_{37}	**M18** → **M26**	7.50×10^{00}	3.10	6584
k_{38}	**M26** → **M27**	1.45×10^{11}	0.42	18 323

which a barrier of 171.0 ± 0.6 kJ mol^{-1} is calculated. On simple thermodynamic grounds the formation of these products was not envisaged to be competitive as the products are computed to lie 25.9 ± 3.7 kJ mol^{-1} above 2MF and hydrogen at 298.15 K, which is likely too endothermic to compete with the exothermic formation of furan and a $\dot{C}H_3$ radical or the 1-butene-1-yl radical and CO.

A 1 → 6 hydrogen atom transfer from the methyl group of **M18** to its oxygen atom to form an alcohol (**M26**), was found to face a very low initial barrier (**TS36**) of 85.0 kJ mol^{-1}. However, the subsequent ring closing reaction *via* **TS38** is too energetic (155.6 ± 0.9 kJ mol^{-1} relative to **M26**) for this reaction channel to be important. The products were computed to lie 36.9 ± 3.7 kJ mol^{-1} above the reactants, and pre- and post-reaction complexes are probably found in the process, but these are not investigated.

RRKM/ME derived product branching ratios from the chemically activated recombination of hydrogen atom with 2MF at C-2 are presented in Fig. 13. Branching ratios for the formation of $\dot{C}_5H_7O$ isomers of the nascent adduct are lumped for clarity in Fig. 13, but product specific rate constants are reported in the ESI.† At high pressures (100 atm) the initially activated well (**M17**) is stabilised up to ≈1200 K, above this temperature the formation and stabilization of linear $\dot{C}_5H_7O$ radicals becomes dominant, thus indicating that ring opening has become competitive with quenching of **M17**. Above 1600 K, furan and a methyl radical and 1-butene-1-yl radical and CO become major products, accounting for 40+% of the chemically activated yield.

These formally direct pathways become increasingly significant with decreasing pressure and in particular the formation of 1-butene-1-yl radical and CO, which must occur through multiple well-skipping reactions, starts to become the dominant bimolecular products of the reaction. The increasing branching ratio for 1-butene-1-yl radical and CO formation corresponds with the lack of quenching of linear $\dot{C}_5H_7O$ radicals with decreasing pressure. On the other hand, the branching ratio for formation of furan and methyl radical shows a lesser

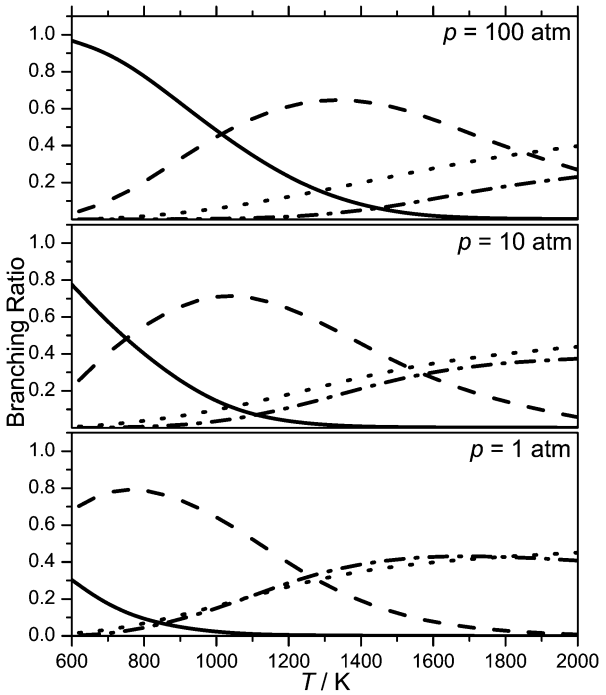

Fig. 13 Major product branching ratios as a function of temperature and pressure from RRKM/ME calculations on the chemically activated recombination of hydrogen atom with 2-methylfuran at C-2. — **M17**, – – ∑ other $\dot{C}_5H_7O$,··· **P10** + **P22**, –·– **P6** + **P23**.

dependency on pressure, owing to the fact it is formed directly from the initial chemically activated species (**M17**).

3.3.2 Addition at C-3 and C-4. Despite the rate constants for the initial hydrogen atom addition reactions at C-3 and C-4 being competitive with addition at C-2 and C-5, subsequent ring opening reactions are less facile, and these pathways are thus uncompetitive with addition at C-2 and C-5. For brevity in the main text, potential energy surfaces for hydrogen atom addition at C-3 and C-4 are described in detail in ESI,† with relevant rate constants also reported therein, k_{41}–k_{52}, and k_{54}–k_{59}.

3.3.3 Addition at C-5. Fig. 14 displays the potential energy surface investigated upon hydrogen atom addition at C-5, with corresponding rate constants reported in Table 7. Ring opening of the adduct occurs through **TS61** with a ring-opening rate constant of a similar order to that computed upon hydrogen atom addition at C-2 (k_{26} and k_{30}). Demethylation of the ring opening product occurs through **TS62** to form vinyl ketene and a methyl radical, in a reaction computed to be endothermic by 176.4 ± 4.7 kJ mol^{-1}. A barrier of 202.0 ± 5.3 kJ mol^{-1} is computed for the process relative to the reactant and 61.7 ± 4.9 kJ mol^{-1} relative to 2MF and a hydrogen atom.

A secondary conformer of the ring opening product (**M43**) can undergo a hydrogen atom transfer reaction with a barrier of 124.6 kJ mol^{-1} (**TS64**) to form an acetonyl-like radical (**M44**), which can undergo β-scission to form ketene and a vinyl propene radical (k_{66}).

Ring closure of **M45** to form a cyclopropanone radical derivative (**M46**) is energetically more favourable than the formation of ketene and a vinyl propene radical, with the transition state for the process (**TS67**) computed to lie only 19.3 ± 3.1 kJ mol^{-1} above 2MF and hydrogen atom. **M46** can rearrange *via* β-scission (**TS68**) to form an aldehydic radical which is capable of eliminating CO through **TS70** to produce the resonantly stabilised butenyl radical (**P36**).

The potential energy surface investigated indicates that hydrogen atom addition at C-5 will proceed with competition

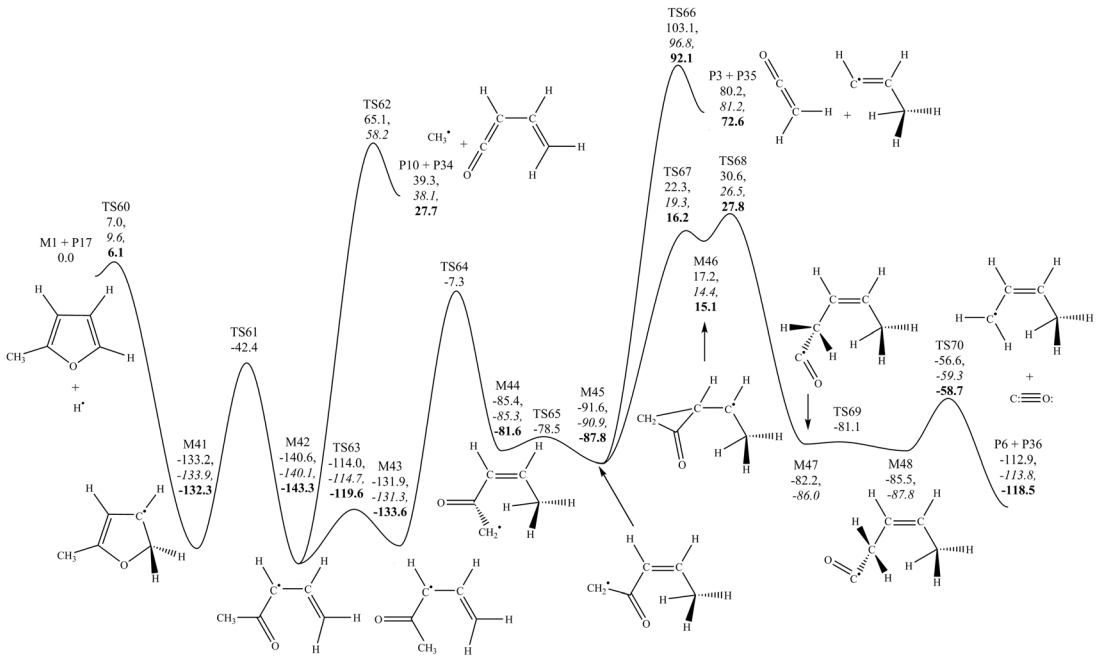

Fig. 14 Potential energy surface for hydrogen atom addition at carbon 5 of 2-methylfuran. CBS-QB3, *CBS-APNO* and **G3** energies in kJ mol^{-1} at 0 K relative to reactants.

Table 7 Arrhenius coefficients of high-pressure limiting rate constants for for reactions relevant to hydrogen atom addition at C-5 of 2-methylfuran. $k(s^{-1}) = AT^n \exp(-E_a/R)$, $AT^n(s^{-1})$, E_a/R (K)

No.	Reaction	A	n	E_a/R (K)
k_{61}	**M41** → **M42**	1.52×10^{12}	0.31	10 931
k_{62}	**M42** → **P10** + **P34**	6.01×10^{14}	0.16	25 568
k_{63}	**M42** → **M43**	3.24×10^{13}	−0.28	3301
k_{64}	**M43** → **M44**	3.64×10^{04}	2.25	11 977
k_{65}	**M44** → **M45**	7.18×10^{12}	−0.16	900
k_{66}	**M45** → **P3** + **P35**	4.29×10^{12}	0.56	23 690
k_{67}	**M45** → **M46**	1.74×10^{13}	−0.42	13 859
k_{68}	**M46** → **M47**	8.27×10^{07}	1.28	940
k_{69}	**M47** → **M48**	5.08×10^{07}	1.25	−313
k_{70}	**M48** → **P6** + **P36**	5.84×10^{10}	0.74	3377

between back dissociation to form 2MF and a hydrogen atom, the endothermic formation of vinyl ketene and a methyl radical in a relatively straightforward 3-step process, and the exothermic formation of CO and $CH_2{=}CH{-}\dot{C}H{-}CH_3$ radical which faces many possible bottlenecks before formation. In terms of the contrast between the addition of a hydrogen atom at the C-2 and C-5 positions of 2-methylfuran, both include a demethylation step with simultaneous formation of a C_4H_4O isomer. The relative stability of the furan ring is reflected in the fact that hydrogen atom addition forming a methyl radical and furan (C-2 addition), faces a much lower barrier than that forming a methyl radical and vinyl ketene (C-5 addition). Likewise, the elimination of CO is a common feature upon hydrogen atom addition at C-2/C-5. In both instances, the CO elimination process is quite rapid despite the differing nature of the co-products formed from these reactions (C-2 addition produces a vinylic radical, C-5 addition produces an allylic radical), and it is the hydrogen atom transfer reactions which precede the decarbonylation step, which will determine whether this process will ultimately occur.

An RRKM/ME analysis, Fig. 15, shows similar trends to those observed for hydrogen atom addition at the C-2 position. At 100 atm collisional deactivation of chemically activated **M41** dominates the product branching fractions up to 1000 K, at which point linear $\dot{C}_5H_7O$ radicals start to form and subsequently stabilize. As a result, the formation of bimolecular products is insignificant at temperatures up to ≈1700 K. At 1 atm the furanyl radical does not persist above 1000 K and above 1300 K, the formation of bimolecular products (vinyl ketene and a methyl radical, 2MF and a hydrogen atom) are dominant.

The formation of vinyl ketene and a methyl radical shows a stronger pressure dependency than the formation of 2MF and a hydrogen atom. Again, this is the result of multiple well skipping reactions occurring at lower pressures to produce the latter. Negligible quantities of CO and $CH_2{=}CH{-}\dot{C}H{-}CH_3$ radical are produced as formally direct products of hydrogen atom addition to 2MF.

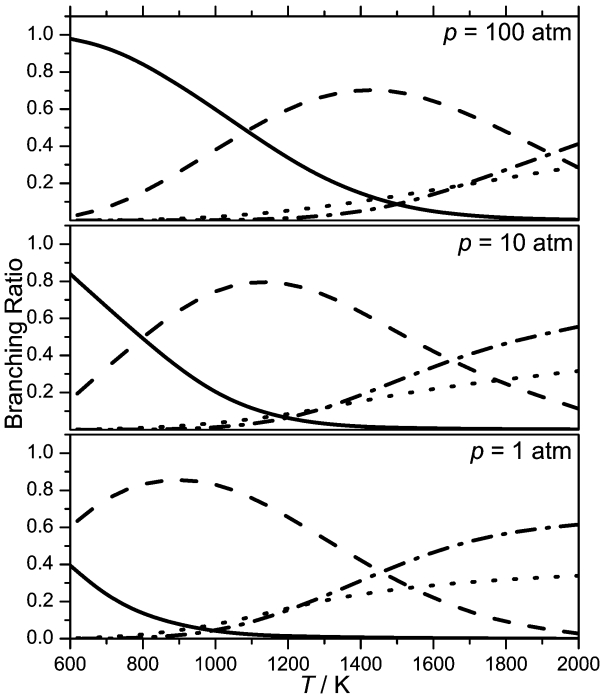

Fig. 15 Major product branching ratios as a function of temperature and pressure from RRKM/ME calculations on the chemically activated recombination of hydrogen atom with 2-methylfuran at C-5. — **M41**, – – ∑ other $\dot{C}_5H_7O$, ··· **M1** + **P17**, –·– **P10** + **P34**.

4 Kinetic modelling

The preceding calculations have been assimilated into a previously published kinetic scheme for 2-methylfuran and 2,5-dimethylfuran combustion by Somers and co-workers[32,70] wherein details of the oxidative reactions are found. Where rate constants are determined at several levels of theory, we utilise the CBS-QB3 calculations in the current work. Furan[18,38] and aromatic[71] mechanisms are also incorporated. The C_0–C_4 sub-mechanism is based on the mechanism described by Healy and co-workers.[72–76] Further validation of this chemistry set is described in the work of Kochar and co-workers[77] and in a recent study of C_1–C_2 hydrocarbon and oxygenated fuels from Metcalfe *et al.*[78] The H_2/O_2 sub-mechanism is adopted from the work of Kéromnès *et al.*[79]

Experimental profiles from Lifshitz *et al.*[14] are presented in Fig. 16 along with numerical modelling results based on the current kinetic mechanism. Some comments on the experimental results are now appropriate before a comparison of modelling predictions with experiment is presented in detail. Mole percents are calculated *via* eqn (1) in accord with the experimental definition,[80] where x_i is the computed mole fraction of a species.

$$\text{Mole}\% = x_i \Big/ \sum_i x_i \qquad (1)$$

Only species which were quantified and included in this mole% calculation experimentally, are included in the corresponding computational results depicted in Fig. 16.

The experimentalists used the chemical thermometer (1,1,1-trifluoroethane) method to determine the temperatures behind the reflected shock wave according to eqn (2) and (3):

$$T = -(E/R) \Big/ \left[\ln\left\{-\frac{\ln(1-\chi)}{At}\right\}\right] \qquad (2)$$

where E and A are the activation energy and pre-exponential factor assumed for the molecular elimination reaction

(CH_3–CF_3 → CH_2═CF_2 + HF) of the chemical thermometer, t is the reaction dwell time and χ is given by:

$$\chi = [CH_2{=}CF_2]_t/([CH_2{=}CF_2]_t + [CH_3{-}CF_3]_t) \quad (3)$$

This makes the determination of the temperature sensitive to both the rate constant used for the decomposition and the determination of the concentrations of the reactant and product of the chemical thermometer. The temperature behind the reflected shock wave was calculated by Lifshitz *et al.* based on a literature assignment of the rate constant[81] for the decomposition of CH_3–CF_3 of $k = 10^{14.51} \exp(-36\,533/T)\ s^{-1}$.

The same chemical thermometer method was employed in the Lifshitz *et al.*[15] study on the thermal decomposition of

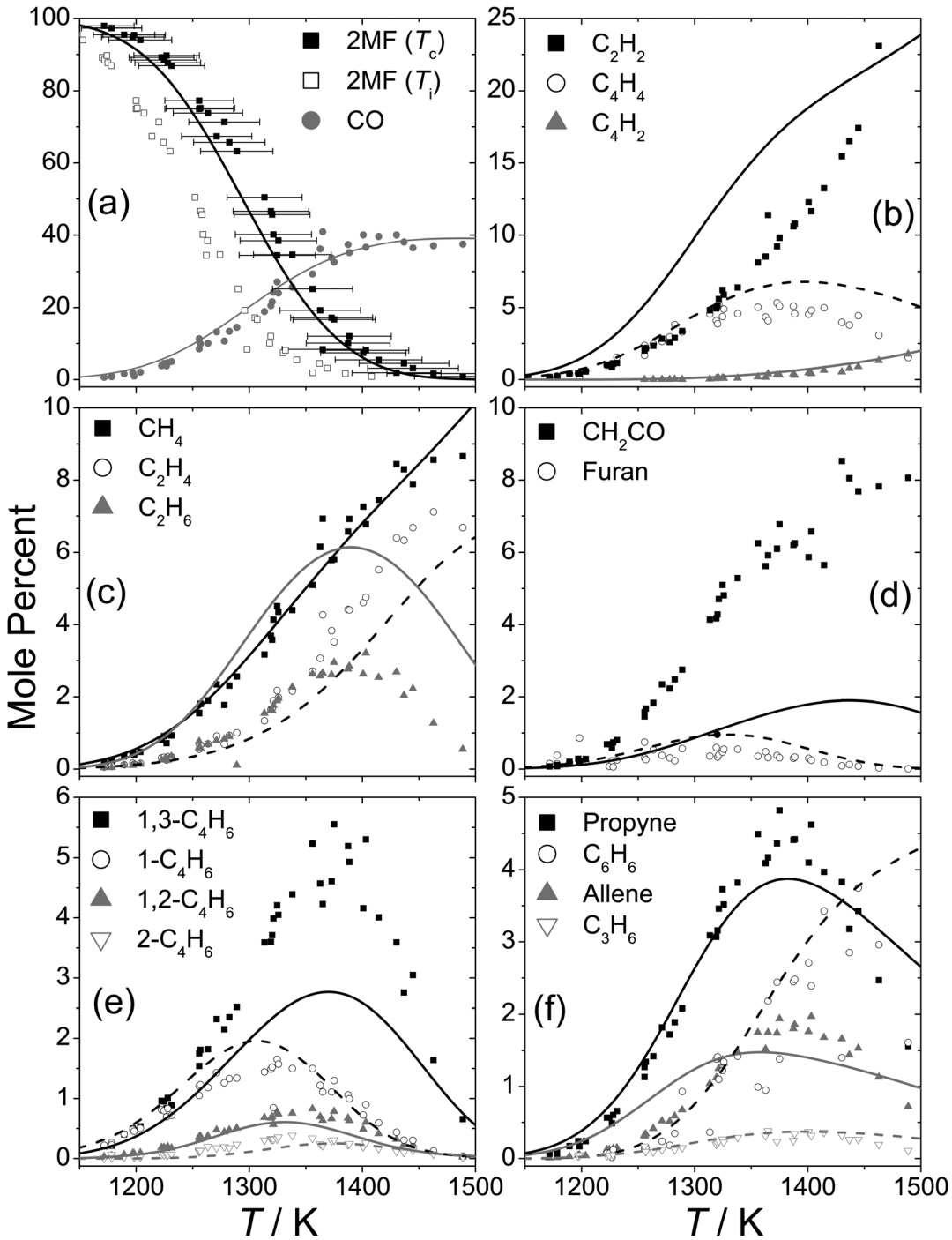

Fig. 16 Experimental speciation profiles for the pyrolysis of 0.5% 2-methylfuran at 2.5 atm and ≈2 ms residence time with modelling predictions (lines). Solid lines correspond with closed symbols and dashed lines with open symbols. T_c = corrected reflected shock temperatures, T_i = original reflected shock temperatures.

2,5-dimethylfuran, although a slightly different rate constant (within 10–20%) was estimated for the thermometer decomposition. Recent experimental and kinetic modelling studies[37,70] have shown that the rate constant assumed by Lifshitz *et al.* in their 2,5-dimethylfuran work was likely in error. Somers *et al.*[70] carried out single pulse shock tube experiments under similar conditions to those of Lifshitz *et al.*[15] where temperatures were determined independent of a chemical thermometer. The results showed that 25DMF underwent decomposition at temperatures up to ≈90 K greater than those determined by Lifshitz *et al.*[15]

Sirjean *et al.*[37] carried out quantum chemical (CBS-QB3) and RRKM/ME calculations to determine the rate constant for the molecular elimination reaction, recommending a rate constant at 2.5 bar of $k = 6.17 \times 10^{13} \exp(-36\,060/T)\ s^{-1}$. At 1200 K, their computed value is up to 3.8 times lower than that assumed by Lifshitz *et al.* in their 2,5-dimethylfuran work,[15] and 3.5 times lower than that assumed in the experiments we are aiming to model here. Sirjean *et al.*[37] corrected the temperature measurements of Lifshitz *et al.* accordingly, with the resultant measurements from Somers *et al.*[70] and the corrected ones of Sirjean *et al.*[37] being within 25 K of each other and in good agreement with kinetic modelling calculations.

We therefore correct the temperature reported by Lifshitz *et al.*[14] for their 2-methylfuran experiments based on the rate constant recommended by Sirjean *et al.*[37] and eqn (2) and (3). The result is a ≈50 K *increase* in the experimental temperature at the lowest conversions of 2-methylfuran, and up to 80 K at the highest temperatures studied. The corrected temperature can be described adequately by $T_c\ (K) = 1.12 \times T_i - 82.54$.

The experimental yields (Fig. 16) of 2MF are presented with temperature uncertainty bars which assume a residual factor of two uncertainty in the recommended rate constant for the thermal decomposition of 1,1,1-TFE, which is reasonable based on the theoretical methods employed therein.[37] Fig. 16(a) also shows the temperature uncorrected yields of 2MF, which clearly lie outside the uncertainty in this updated temperature profile.

In order to obtain better agreement with the corrected 2MF and methane profiles, we have reduced the rate constant for hydrogen atom abstraction by methyl radical from the alkyl side chain of 2MF, $k_{CH_3-C_2}$(QB3), by a factor of two, which is within the theoretical uncertainty. The rate constant for hydrogen atom abstraction by hydrogen atom, k_{H-C_2}(QB3), has been increased by a factor of two in order to retain agreement with laminar burning velocity measurements,[32] as was carried out in the previous kinetic modelling study of Somers *et al.*[32] The rate constant for this reaction shows little sensitivity to the pyrolysis results described here and our predictions of the fuel conversion in Fig. 16(a) are well within the experimental uncertainty.

Lifshitz *et al.*[14] originally recommended a pseudo-first order rate constant of $9.71 \times 10^{13} \exp(-34\,400/T)\ s^{-1}$ for the thermal decomposition of 2MF in this temperature and pressure regime. After correction of their data, we arrive at $8.41 \times 10^{13} \exp(-34\,450/T)\ s^{-1}$ with our kinetic model predicting a rate constant of $1.97 \times 10^{14} \exp(-35\,071/T)\ s^{-1}$. For all three derived rate constants, the activation energies are of the order of ≈286–291 kJ mol^{-1}, which corresponds closely with the barrier heights calculated for the 3 → 2 and 4 → 5 hydrogen atom shift reactions shown to be the dominant unimolecular decomposition pathways for 2MF in previous sections. This is an interesting result, as free radical reactions are found to be important in the consumption of the reactant species. One might expect the activation energy to be smaller than the activation energies for the primary unimolecular initiation pathways but the thermal decomposition of 2MF seems to obey first order kinetics quite well in this temperature range.

The fate of the oxygen containing fragments of the fuel are of obvious interest and other than 2MF, only three species were experimentally measured which contained an oxygen atom; CO, ketene and furan. CO, which was found to be the primary decomposition product, was detected in yields of up to 40%, and is well-predicted by our kinetic model. Its formation is well rationalised within our quantum chemical calculations through multiple channels. Opening of the furan ring, followed by a hydrogen transfer reaction and CO elimination is common to the unimolecular decomposition reactions of the fuel and the primary fuel radical, and is also seen after hydrogen atom addition reactions. The reaction $CH_3\text{–}\dot{C}{=}O \rightarrow CO + \dot{C}H_3$ is also an important source of CO, with the majority of the $CH_3\text{–}\dot{C}{=}O$ radical formed in a 1 : 1 ratio with $CH_2{=}C{=}\dot{C}H$ radical from the decomposition of **M9**.

Ketene yields of up to 8% were implied from experiment but the determination of its concentrations proved difficult due to analytical issues. A series of isolated experiments were performed by Lifshitz *et al.*[14] where small quantities of methanol were added to the post-shock mixture in order convert ketene to the more readily quantifiable methyl acetate. Methyl acetate was subsequently identified although its concentrations could not be quantitatively determined. It was therefore assumed that if ketene was formed in the same unimolecular process as propyne and allene, its concentrations should equal the sum of the C_3H_4 isomers. Despite multiple pathways (Fig. 2 and 14, Fig. S1 and S2 of ESI†) leading to the production of ketene within our assembled reaction scheme, its formation is consistently found to be non-competitive with alternate pathways.

We find vinyl ketene, which went experimentally undetected by Lifshitz[14] but which was identified in 2MF flames,[69] to be a major product upon hydrogen atom addition at C-5 of the furan ring. Computed vinyl ketene yields are in good agreement with the experimentally estimated ketene concentrations if this undetected species is incorporated into our mole% calculation, Fig. 17. Vinyl ketene may therefore account for the missing carbon and oxygen which the experimentalists assumed would be found in ketene.

Furan yields are well-predicted and its formation pathway was clearly rationalised in a previous work by Simmie and Metcalfe.[25] However, the ring opening step presented in Fig. 11 is central to the accurate prediction of its yields shown in Fig. 16(d), with the exclusion of this process resulting in over-prediction of the experimental yield.

The yield of methane, which is primarily formed by hydrogen atom abstraction from the alkyl side chain by methyl radical, is also well-predicted although yields of ethane, which is formed from methyl radical self-recombination, is over-predicted by

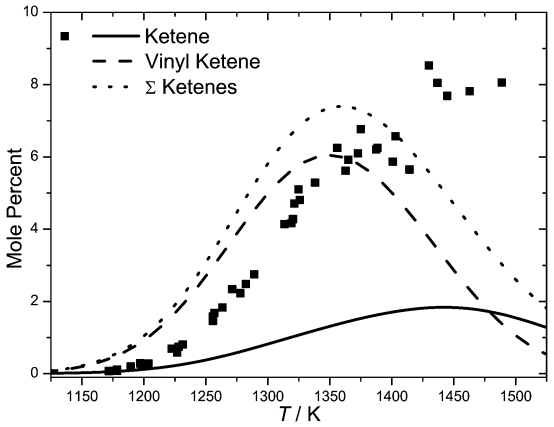

Fig. 17 Experimentally estimated yields[14] (see text) of ketene (symbols) with computational yields of ketene and vinyl ketene.

the mechanism. Ethylene is formed from the decomposition of ethyl radical which is in turn formed from the decomposition of **P23** and from the reaction $C_2H_6 + \dot{C}H_3 = \dot{C}_2H_5 + CH_4$. Yields of the C_4H_6 isomers 1-butyne, 2-butyne, 1,2-butadiene and 1,3-butadiene are all reasonably-well estimated by our kinetic mechanism.

Like ketene, many pathways leading to the formation of propyne were identified in our quantum calculations (k_4, k_{13}, k_{47}, k_{66}) but none were found to be competitive. Nonetheless, propyne, allene, and benzene yields are all accounted for. The former are produced *via* abstraction by propargyl radical from the alkyl side chain of 2MF, and the latter *via* the recombination of propargyl radicals. It is worth noting that propargyl radical was identified by Grela *et al.*[16] in the thermal decomposition of 2MF, based on the presence of its ion at *m*/*z* 39 in their MS analysis. Our work proposes two clear channels to its formation from 2MF *via* the reactions sequences (a) 2MF → **M6** → CO + CH≡C–CH_2–CH_3 → $\dot{C}H_3$ + CH_2=C=$\dot{C}$H and (b) 2MF → **M9** → CH_3–$\dot{C}$=O + CH_2=C=$\dot{C}$H.

The decomposition of *n*-butadienyl radical, which is the primary product of the decomposition of the 2-furanylmethyl radical, Fig. 7, accounts for the acetylene and vinylacetylene concentrations detected experimentally. Vinylacetylene predictions are in excellent agreement with experiment, although acetylene yields are consistently over-estimated, possibly indicating refinements to the kinetics of *n*-butadienyl radical decomposition are necessary.

5 Conclusions

This work presents a comprehensive investigation of the potential energy surfaces for the pyrolysis reactions of the biofuel candidate 2-methylfuran. Kinetics for the thermal unimolecular reactions of 2-methylfuran and the 2-furanylmethyl radical, the chemically activated recombination of hydrogen atoms with 2-methylfuran and several hydrogen atom abstraction processes have been investigated. Canonical and microcanonical rate theories have been employed to determine rate constants as a function of temperature and pressure (if applicable) for each reaction pathway.

Unimolecular decomposition is initiated primarily by hydrogen shift reactions routed through β-carbene intermediates to form stable acyclic intermediates which further decompose to either 1-butyne and CO, or acetyl and propargyl radicals. As temperatures approach 2000 K, the formation of 1,2-butadiene and CO, ketene and propyne, and 2-furanylmethyl radical and a hydrogen atom become competitive. The decomposition of the 2-furanylmethyl radical is shown to proceed through C–O bond cleavage which opens the furan ring. Subsequent hydrogen atom transfer and α-scission leads to the formation of the dominant products, CO and the *n*-butadienyl radical. Hydrogen atom addition to carbon atoms adjacent to the oxygen of the furan ring are kinetically favoured over addition to atoms remote from the oxygen moiety. In terms of bimolecular products, hydrogen atom addition results predominantly in the formation of furan and a methyl radical, 1-butene-1-yl radical and CO, and vinyl ketene and a methyl radical.

The calculated rate constants are incorporated into a previously published oxidative mechanism for 2-methylfuran[32] and 2,5-dimethylfuran[70] which is then compared with experimental speciation profiles[14] recorded for the pyrolysis of 2-methylfuran. Once the experimental measurements are corrected for an erroneous temperature determination the agreement between theory and experiment is overall quite good, thus giving some credibility to the proposed pyrolysis mechanism and kinetics. The mechanism is also compared to literature oxidation experiments of 2MF in the ESI,† with good performance observed against all experimental targets.

The fundamental molecular data provided in this study should be of interest to those who wish to carry out RRKM/ME calculations on 2-methylfuran in the future with the chemical mechanism being of utility to those modelling the combustion behavior of 2-methylfuran under pyrolysis and oxidative conditions. Furan, 2-methylfuran and 2,5-dimethylfuran are also know intermediates and model compounds considered in the pyrolysis of biomass[82,83] and coals,[17] and the kinetic scheme developed herein is likely to be useful in kinetic modelling work in these areas.

Acknowledgements

We would like to acknowledge the support of Science Foundation Ireland under grant number [08/IN1./I2055] as part of their Principal Investigator Awards. We acknowledge the provision of computational resources from the e-Irish National Infrastructure programme, e-INIS, and the Irish Centre for High-End Computing, ICHEC. We thank Prof. John Barker and Dr Gabriel da Silva for useful discussions on the Multiwell code and the latter again for sharing with us the Speed v0.72 code for automatic generation of potential energy surfaces.

References

1 Energy Policy Network for the 21st Centry. Renewables 2013 Global Status Report. http://www.ren21.net/REN21Activities/GlobalStatusReport.aspx, accessed October 21, 2013.
2 J. R. Regalbuto, *Science*, 2009, **325**, 822–824.

3 Y. Román-Leshkov, C. J. Barrett, Z. Y. Liu and J. A. Dumesic, *Nature*, 2007, **447**, 982–985.
4 H. Zhao, J. E. Holladay, H. Brown and Z. C. Zhang, *Science*, 2007, **316**, 1597–1599.
5 J. B. Binder and R. T. Raines, *J. Am. Chem. Soc.*, 2009, **131**, 1979–1985.
6 Y. Su, H. M. Brown, X. Huang, X. Zhou, J. E. Amonette and Z. C. Zhang, *Appl. Catal., A*, 2009, **361**, 117–122.
7 A. A. Rosatella, S. P. Simeonov, R. F. M. Frade and C. M. Afonso, *Green Chem.*, 2011, **13**, 754–793.
8 F. Geilen, T. vom Stein, B. Engendahl, S. Winterle, M. Liauw, J. Klankermayer and W. Leitner, *Angew. Chem., Int. Ed.*, 2011, **50**, 6831–6834.
9 S. Zhong, R. Daniel, H. Xu, J. Zhang, D. Turner, M. L. Wyszynski and P. Richards, *Energy Fuels*, 2010, **24**, 2891–2899.
10 R. Daniel, G. Tian, H. Xu, M. L. Wyszynski, X. Wu and Z. Huang, *Fuel*, 2011, **90**, 449–458.
11 M. Thewes, M. Muether, S. Pischinger, M. Budde, A. Sehr, P. Adomeit and J. Klankermayer, *Energy Fuels*, 2011, **25**, 5549–5561.
12 C. Wang, H. Xu, R. Daniel, A. Ghafourian, J. M. Herreros, S. Shuai and X. Ma, *Fuel*, 2013, **103**, 200–211.
13 A. Lifshitz, M. Bidani and S. Bidani, *J. Phys. Chem.*, 1986, **90**, 5373–5377.
14 A. Lifshitz, C. Tamburu and R. Shashua, *J. Phys. Chem. A*, 1997, **101**, 1018–1029.
15 A. Lifshitz, C. Tamburu and R. Shashua, *J. Phys. Chem. A*, 1998, **102**, 10655–10670.
16 M. A. Grela, V. T. Amorebieta and A. J. Colussi, *J. Phys. Chem.*, 1985, **89**, 38–41.
17 O. S. L. Bruinsma, P. J. J. Tromp, H. J. J. de Sauvage Nolting and J. A. Moulijn, *Fuel*, 1988, **67**, 334–340.
18 K. Sendt, G. B. Backsay and J. C. Mackie, *J. Phys. Chem. A*, 2000, **104**, 1861–1875.
19 P. P. Organ and J. C. Mackie, *J. Chem. Soc., Faraday Trans.*, 1991, **87**, 815–823.
20 R. Liu, X. Zhou and L. Zhai, *J. Comput. Chem.*, 1998, **19**, 240–249.
21 R. Liu, X. Zhou and T. Zuo, *Chem. Phys. Lett.*, 2000, **325**, 457–464.
22 J. M. Simmie and H. J. Curran, *J. Phys. Chem. A*, 2009, **113**, 5128–5137.
23 D. Feller and J. M. Simmie, *J. Phys. Chem. A*, 2013, **116**, 11768–11775.
24 M. A. V. Ribeiro da Silva and L. M. P. F. Amaral, *J. Therm. Anal. Calorim.*, 2010, **100**, 375–380.
25 J. M. Simmie and W. K. Metcalfe, *J. Phys. Chem. A*, 2011, **115**, 8877–8888.
26 X. Wu, Z. Huang, T. Yuan, K. Zhang and L. Wei, *Combust. Flame*, 2009, **156**, 365–376.
27 P. Friese, T. Bentz, M. Olzmann, J. Simmie, Proceedings of the European Combustion Meeting, 2011.
28 P. Friese, J. M. Simmie and M. Olzmann, *Proc. Combust. Inst.*, 2013, **34**, 233–239.
29 B. Sirjean and R. Fournet, *Phys. Chem. Chem. Phys.*, 2013, **15**, 596–611.
30 B. Sirjean and R. Fournet, *Proc. Combust. Inst.*, 2013, **34**, 241–249.
31 B. Sirjean and R. Fournet, *J. Phys. Chem. A*, 2012, **116**, 6675–6684.
32 K. P. Somers, J. M. Simmie, F. Gillespie, U. Burke, J. Connolly, W. K. Metcalfe, F. Battin-Leclerc, P. Dirrenberger, O. Herbinet, P.-A. Glaude and H. J. Curran, *Proc. Combust. Inst.*, 2013, **34**, 225–232.
33 A. Y. Chang, J. W. Bozzelli and A. M. Dean, *Z. Phys. Chem.*, 2000, **214**, 1533–1568.
34 J. W. Bozzelli, A. M Chang and A. M. Dean, *Int. J. Chem. Kinet.*, 1997, **29**, 161–170.
35 A. C. Davis and S. M. Sarathy, *J. Phys. Chem. A*, 2013, **117**, 7670–7685.
36 L.-S. Tran, C. Togbé, D. Liu, D. Felsmann, P. Oßwald, P.-A. Glaude, R. Fournet, B. Sirjean, F. Battin-Leclerc and K. Kohse-Höinghaus, *Combust. Flame*, 2013, DOI: 10.1016/j.combustflame.2013.05.027.
37 B. Sirjean, R. Fournet, P.-A. Glaude, F. Battin-Leclerc, W. Wang and M. A. Oehlschlaeger, *J. Phys. Chem. A*, 2013, **117**, 1371–1392.
38 Z. Tian, T. Yuan, R. Fournet, P.-A. Glaude, B. Sirjean, R. Battin-Leclerc, K. Zhang and F. Qi, *Combust. Flame*, 2011, **158**, 756–773.
39 L. Wei, C. Tang, X. Man and Z. Huang, *Energy Fuels*, 2013, **27**, 7809–7816.
40 A. D. Becke, *J. Chem. Phys.*, 1993, **98**, 5648–5652.
41 C. Lee, W. Yang and R. G. Parr, *Phys. Rev. B: Condens. Matter Mater. Phys.*, 1988, **37**, 785–789.
42 H. P. Hratchian and H. B. Schlegel, *J. Chem. Theory Comput.*, 2005, **1**, 61–69.
43 J. A. Montgomery, M. J. Frisch, J. W. Ochterski and G. A. Petersson, *J. Chem. Phys.*, 2000, **112**, 6532–6542.
44 J. W. Ochterski, G. A. Petersson and J. A. Montgomery, *J. Chem. Phys.*, 1996, **104**, 2598–2619.
45 L. A. Curtiss, K. Raghavachari, P. C. Redfern, V. Rassolov and J. A. Pople, *J. Chem. Phys.*, 1998, **109**, 7764–7776.
46 J. M. Simmie, K. P. Somers, W. K. Metcalfe and H. J. Curran, *J. Chem. Thermodyn.*, 2013, **58**, 117–128.
47 M. J. Frisch, G. W. Trucks, H. B. Schlegel, G. E. Scuseria, M. A. Robb, J. R. Cheeseman, J. A. Montgomery Jr., T. Vreven, K. N. Kudin, J. C. Burant, J. M. Millam, S. S. Iyengar, J. Tomasi, V. Barone, B. Mennucci, M. Cossi, G. Scalmani, N. Rega, G. A. Petersson, H. Nakatsuji, M. Hada, M. Ehara, K. Toyota, R. Fukuda, J. Hasegawa, M. Ishida, T. Nakajima, Y. Honda, O. Kitao, H. Nakai, M. Klene, X. Li, J. E. Knox, H. P. Hratchian, J. B. Cross, V. Bakken, C. Adamo, J. Jaramillo, R. Gomperts, R. E. Stratmann, O. Yazyev, A. J. Austin, R. Cammi, C. Pomelli, J. W. Ochterski, P. Y. Ayala, K. Morokuma, G. A. Voth, P. Salvador, J. J. Dannenberg, V. G. Zakrzewski, S. Dapprich, A. D. Daniels, M. C. Strain, O. Farkas, D. K. Malick, A. D. Rabuck, K. Raghavachari, J. B. Foresman, J. V. Ortiz, Q. Cui, A. G. Baboul, S. Clifford, J. Cioslowski, B. B. Stefanov, G. Liu, A. Liashenko, P. Piskorz, I. Komaromi, R. L. Martin,

D. J. Fox, T. Keith, M. A. Al-Laham, C. Y. Peng, A. Nanayakkara, M. Challacombe, P. M. W. Gill, B. Johnson, W. Chen, M. W. Wong, C. Gonzalez and J. A. Pople, *Gaussian 03, Revision E., 01, and Gaussian 09, Revision C.01*, Gaussian, Inc., Wallingford, CT, 2004.

48 MultiWell-2013 Software, Jan 2013, designed and maintained by J. R. Barker with contributors N. F. Ortiz, J. M. Preses, L. L. Lohr, A. Maranzana, P. J. Stimac, T. L. Nguyen, and T. J. Dhilip Kumar, University of Michigan, Ann Arbor, MI; http://aoss.engin.umich.edu/multiwell/.

49 (*a*) J. R. Barker, *Int. J. Chem. Kinet.*, 2001, **33**, 232–245; (*b*) J. R. Barker, *Int. J. Chem. Kinet.*, 2001, **33**, 246–261; (*c*) J. R. Barker, *Int. J. Chem. Kinet.*, 2009, **41**, 748–763.

50 S. J. Pinches and G. da Silva, *Int. J. Chem. Kinet.*, 2013, **45**, 387–396.

51 V. Mokrushin and W. Tsang, *ChemRate version 1.5.8*, NIST, Gaithersburg, MD 20899, 2013, http://mokrushin.com/ChemRate/chemrate.html, accessed June 21 2013.

52 D. Polino and C. Cavalotti, *J. Phys. Chem. A*, 2011, **115**, 10281–10289.

53 G. da Silva, J. A. Cole and J. W. Bozzelli, *J. Phys. Chem. A*, 2009, **113**, 6111–6120.

54 C. Cavallotti and D. Polino, *Proc. Combust. Inst.*, 2013, **34**, 557–564.

55 G. da Silva and A. J. Trevitt, *Phys. Chem. Chem. Phys.*, 2011, **13**, 8940–8952.

56 G. da Silva, *Chem. Phys. Lett.*, 2009, **474**, 13–17.

57 G. da Silva, J. A. Cole and J. W. Bozzelli, *J. Phys. Chem. A*, 2010, **114**, 2275–2283.

58 G. da Silva, M. Rafiq Hamdan and J. W. Bozzelli, *J. Chem. Theory Comput.*, 2009, **5**, 3185–3194.

59 J. A. Miller and S. J. Klippenstein, *J. Phys. Chem. A*, 2013, **117**, 2718–2727.

60 A. W. Jasper, J. A. Miller and S. J. Klippenstein, *J. Phys. Chem. A*, 2013, **117**, 12243–12255.

61 H. Hippler, J. Troe and H. J. Wendelken, *J. Chem. Phys.*, 1983, **78**, 6709–6717.

62 R. J. Kee, M. E. Coltrin, P. Glarborg, *Chemically Reacting Flow Theory and Practice*, John Wiley & Son, Inc., New Jersey, 1st edn, 2003, pp. 496–499.

63 W. M. Haynes, Critical Constants of Organic Compounds, *CRC Handbook of Chemistry and Physics*, CRC Press, Boca Raton, Florida, 91st edn, p. 67.

64 X. Ma, C. Jian, H. Xu, H. Ding, S. Shuai and H. Ding, *Energy Fuels*, 2013, **27**, 6212–6221.

65 Chemkin-Pro, Reaction Design Inc., San Diego, Calif., 2010.

66 L. B. Harding and S. J. Klippenstein, *J. Phys. Chem. A*, 2007, **111**, 3789–3801.

67 Y.-R. Luo, *Comprehensive Handbook of Chemical Bond Energies*, CRC Press, Boca Raton, FL, 2007, p. 41.

68 H. Wang and K. Brenzinsky, *J. Phys. Chem. A*, 1998, **102**, 1530–1541.

69 L. Wei, Z. Li, L. Tong, Z. Wang, H. Jin, M. Yao, Z. Zheng, C. Wang and H. Xu, *Energy Fuels*, 2012, **26**, 6651–6660.

70 K. P. Somers, J. M. Simmie, F. Gillespie, C. Conroy, G. Black, W. K. Metcalfe, F. Bttin-Leclerc, P. Dirrenberger, O. Herbinet, P.-A. Glaude, P. Dagaut, C. Togbé, K. Yasunaga, R. X. Fernandes, C. Lee, R. Tripathi and H. J. Curran, *Combust. Flame*, 2013, **160**, 2291–2318.

71 W. K. Metcalfe, S. Dooley and F. L. Dryer, *J. Phys. Chem. A*, 2011, **25**, 4915–4936.

72 D. Healy, N. S. Donato, C. J. Aul, E. L. Petersen, C. M. Zinner, G. Bourque and H. J. Curran, *Combust. Flame*, 2010, **157**, 1526–1539.

73 N. Donato, C. Aul, E. Petersen, C. Zinner, H. Curran and G. Bourque, *J. Eng. Gas Turbines Power*, 2010, **132**, 051502.

74 D. Healy, N. S. Donato, C. J. Aul, E. L. Petersen, C. M. Zinner, G. Bourque and H. J. Curran, *Combust. Flame*, 2010, **157**, 1540–1551.

75 D. Healy, D. M. Kalitan, C. J. Aul, E. L. Petersen, G. Bourque and H. J. Curran, *Energy Fuels*, 2010, **24**, 1521–1528.

76 D. Healy, M. M. Kopp, N. L. Polley, E. L. Petersen, G. Bourque and H. J. Curran, *Energy Fuels*, 2010, **24**, 1617–1627.

77 Y. Kochar, J. Seitzman, T. Lieuwen, W. K. Metcalfe, S. M. Burke, H. J. Curran, M. Krejci, W. Lowry, E. Petersen, G. Bourque, 2011, ASME Paper GT, 2011, 45122, 56th ASME Turbo Expo.

78 W. K. Metcalfe, S. M. Burke, S. S. Ahmed and H. J. Curran, *Int. J. Chem. Kinet.*, 2013, **45**, 638–675.

79 A. Kéromnès, W. K. Metcalfe, K. A. Heufer, N. Donohoe, A. K. Das, C. J. Sung, J. Herzler, C. Naumann, P. Griebel, O. Mathieu, M. C. Krejci, E. L. Petersen, W. J. Pitz and H. J. Curran, *Combust. Flame*, 2013, **160**, 995–1011.

80 A. Lifshitz, M. Bidani and S. Bidani, *J. Phys. Chem.*, 1986, **90**, 3422–3429.

81 A. S. Rodgers and W. G. F. Ford, *Int. J. Chem. Kinet.*, 1973, **5**, 965–975.

82 E. Ranzi, A. Cuoci, T. Faravelli, A. Frassoldati, G. Migliavacca, S. Pierucci and S. Sommariva, *Energy Fuels*, 2008, **22**, 4292–4300.

83 K. Norinaga, T. Shoji, S. Kudo and J. Hayashia, *Fuel*, 2013, **103**, 141–150.